Pan African University
Institute of Water and Energy Sciences

PAN AFRICAN UNIVERSITY
INSTITUTE FOR WATER AND ENERGY SCIENCES
(including CLIMATE CHANGE)

Master Dissertation

Submitted in partial fulfillment of the requirements for the Master degree in

Energy Engineering

Presented by

Zvirevo CHISADZA

Optical Characterisation and Modelling of Films and Organic Solar Cells

Defended on 03/09/2018 Before the Following Committee:

Chair	Prof. Mustapha Benmouna	University of Tlemcen
Supervisor	Dr. Harald Hoppe	CEEC, Jena, Germany
External Examiner	Prof. Amine Boudghene Stambouli	University of Oran
Internal Examiner	Prof. Latifa Negadi	University of Tlemcen

DECLARATION

I, Zvirevo Chisadza do hereby declare that this thesis represents my personal work, realized to the best of my knowledge. I also declare that all information, material and results from other works presented here, have been fully cited and referenced in accordance with the academic rules and ethics.

Signature:

Zvirevo Chisadza

Date: 19.08.2018

CERTIFICATION

I hereby certify that this master thesis by **Zvirevo CHISADZA**, an Energy Engineering master student of Pan African University Institute of Water and Energy Sciences (including climate change) (PAUWES), Tlemcen, Algeria was carried out under my supervision.

.....

Supervisor

Dr. Harald Hoppe

29.08.18

.....

Date

.....

Professor Abdellatif ZERGA

Director PAUWES

.....

Date

ACKNOWLEDGMENTS

I would like to acknowledge the African Union Commission (AUC) for the USD $3000 research grant that enabled me to conduct research on this thesis. I would also like to acknowledge my supervisor Dr. Harald Hoppe for the guide and support he gave for this thesis. I would also like to appreciate the help from Dr. Rolf Oettking for his help on optical modelling using CODE software. Lastly, my acknowledgements go to my colleagues at the Center for Energy and Environmental Chemistry (CEEC Jena) for their collective support and motivation on my work. My friend Chikezie Ugokwe has given me both help and motivation throughout the master thesis time and this cannot go unappreciated.

ABSTRACT

This thesis describes the optical characterization and modelling of films and organic solar cells. Different organic solar cell layer films were deposited on glass substrates and their optical constants were determined. Optical characterization involved reflection and transmission measurements for each layer film. Reflection and transmission measurements were used for fitting dielectric functions of the films using CODE software in order to determine complex optical constants for each layer material. Bruggeman's effective medium approach was used to obtained optical constants of two-phase composite materials from their constituent materials. Obtained optical constants for each organic solar cell layer were used to simulate the whole organic solar cell multilayer system using the transfer matrix formalism (TMF). The transfer matrix method used considers the interference in the multilayer system and the multiple reflection and transmission in both the millimeter sized glass substrate and the nanometer sized layers. From the simulation, a simplified method of determining optimal active layer thickness, maximum current density and absorption in the organic solar cell photoactive layer was formulated. Results produced help understand the optical behaviour of light interaction with an organic solar cell multilayer system and can be used in the performance improvement of organic solar cells.

RESUME

Cette thèse décrit la caractérisation optique et la modélisation de films et de cellules photovoltaïques organiques. Différents films de cellules photovoltaïques ont été déposés sur des substrats de verre et leurs constantes optiques ont été déterminées. La caractérisation optique implique des mesures de réflexion et de transmission pour chaque film. Les mesures de réflexion et de transmission ont été utilisées pour ajuster les fonctions diélectriques des films en utilisant le logiciel CODE afin de déterminer la constante optique complexe pour chaque matériau.

L'approche efficace moyenne de Bruggeman a été utilisée pour obtenir les constantes optiques de matériau composite à deux phases de leur matériau constitutif. Les constantes optiques obtenues pour chaque couche ont été utilisées pour simuler le système complet des cellules photovoltaïques organiques multicouches en appliquant le formalisme de la matrice de transfert (TMF). La méthode de la matrice de transfert utilisée prend en compte l'interférence dans le système multicouche et les multiples réflexions et transmissions dans le substrat de verre millimétrique et les couches nanométriques. De la simulation, une méthode simplifiée pour déterminer l'épaisseur optimale de la couche active, la densité de courant maximale et l'absorption maximale dans la couche active de la cellule photovoltaïque organique a été formulée. Les résultats produits aident à comprendre le comportement optique de l'interaction de la lumière avec une cellule photovoltaïque multicouche et peuvent être utilisés pour améliorer les performances de ces dernières.

TABLE OF CONTENTS

LIST OF FIGURES

LIST OF TABLES

LIST OF ABBREVIATIONS AND SYMBOLS

AC	Alternative current
AFM	Atomic force microscopy
AM1.5	Air mass 1.5
BHJ	Bulk heterojunction
CB	Chlorobenzene
D	The electric displacement
DC	Direct current
EQE	External quantum efficiency
ETL	Electron transport layer
εo	Vacuum permittivity
ε_b	Dielectric background constant
ε'	Imaginary part of the complex dielectric function
ε''	real part of the complex dielectric function
FF	Fill factor
E	Electric field
H	The magnetic field induction
HOMO	Highest occupied molecular orbital
HTL	Hole transport layer
IQE	Internal quantum efficiency
ITIC	3,9-bis(2-methylene-(3-(1,1-dicyanomethylene)-indanone))-5,5,11,11-tetrakis(4-hexylphenyl)-dithieno[2,3-d:2',3'-d']-s-indaceno[1,2-b:5,6-b']dithiophene
ITO	Indium tin oxide
IV	Current-voltage
Jsc	Short circuit current density
k	Extinction coefficient (imaginary part of the refractive index)
n	real part of refractive index
LUMO	Lowest unoccupied molecular orbital

ñ	Complex refractive index
ηabs	Number of photons absorbed by the active layer
q	Charge of electron
P	The Electric Polarisation
OPV	Organic photovoltaic
P3HT	Poly(3-hexylthiophene)
PBDB-T	poly[(2,6-(4,8-bis(5-(2-ethylhexyl)thiophen-2-yl)-benzo[1,2-b:4,5-b']dithiophene))-alt-(5,5-(1',3'-di-2-thienyl-5',7'-bis(2-ethylhexyl)benzo[1',2'-c:4',5'-c']dithiophene-4,8-dione)]
PCBM	[6,6]-phenyl-C61-butyric acid methyl ester
PCE	Power conversion efficiency
PEDOT:PSS	Poly(3,4-ethylenedioxythiophene):poly(styrene) sulfonate
PL	Photoluminescence
ρ	Charge density
R	Reflection
RWCA	Rigorous Wave Coupled Analysis
CODE	Coating Designer
T	Transmission
rs	Fresnel reflectance equation at the interface of normal incident for electric wave on the surface.
rp	Fresnel reflectance equation at the interface of parallel incident for electric wave on the surface.
TMF	Transfer matrix formalism
ts	Fresnel transmittance equation at the interface of normal incident for electric wave on the surface.
tp	Fresnel transmittance equation at the interface of parallel incident for electric wave on the surface.
UV-vis	UV-visible spectroscopy
Voc	Open circuit voltage

1. INTRODUCTION

This Section describes the background behind organic solar cells, their optical properties and a brief literature on optical characterization and modelling of organic solar cell materials. Lastly a research plan for this thesis is outlined giving the key blocks of the thesis work.

1.1. Background information

The world is faced with an energy crisis due to depletion of fossil fuels and concerns regarding greenhouse gas emissions. Rapid population growth, industrialization, urbanization and growth in technology trends have led to a sharp increase in global energy consumption. This growing world population and related energy consumption coupled together with the greenhouse gas emissions due to fossil-based energy sources pose a threat to the current and future human generations. According to the World Energy Council [1], world energy consumption will be growing significantly in the coming decades. To illustrate this, three different scenarios were evaluated from 1990 to 2100 (see Figure 1.1) where A is the most pessimistic scenario with high economic growth rates and C is the optimistic and ecologically driven scenario type.

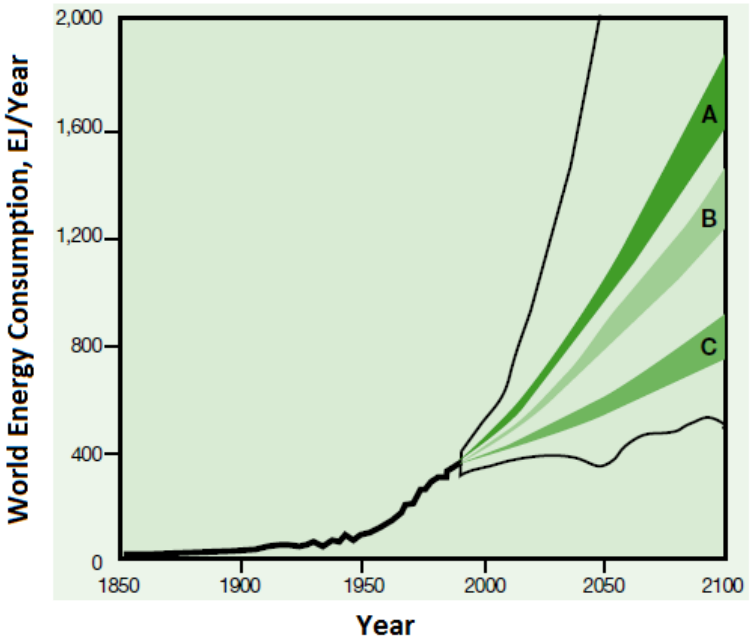

Figure 1.1 Global primary energy requirements from 1850-1990, and the three scenarios (A. B and C) predicting world energy requirements from 1990-2100 [1].

From the results of Figure 1 above and many other cases pointing to the need for scaling up energy production, it can be concluded without doubt that there is a strong need for exploring means of increasing the world energy production. However, it is worth attention to note that satisfying this rapid growth in energy consumption with fossil fuels can have a significant impact on the climate change. Needless to say that there is a strong demand and potential for renewable alternatives which include wind, solar, biomass, hydropower and geothermal energy. Of these renewable energy sources, solar energy is an abundant and virtually eternal renewable energy source. This thesis report focusses on solar energy and specifically organic solar cells.

1.2. Introduction to Solar Cells and Organic Photovoltaics

A solar cell is basically an electronic device that converts sunlight into electricity. Solar cells can be broadly categorized into inorganic and organic solar cells. Inorganic solar cells are made from the conventional silicon materials. They are built from intrinsic semiconductor materials such as silicon (Si) and germanium (Ge) that are usually doped with group III or group V donor or acceptor materials to improve their electrical conductivity [2]. Inorganic photovoltaic devices produce free charge carriers after the

absorption of light, while in organic photovoltaics (OPVs) an exciton (an electron–hole pair bound together by electrostatic energy) is generated after absorbing a photon [3].

An organic solar cell sometimes referred to as polymer or plastic solar cell is defined by applying semiconducting conjugated polymers as active components in the photocurrent generation and power conversion process within thin film photovoltaic devices that convert solar light into electrical energy. Organic solar cells, broadly referred to as organic photovoltaic (OPV) devices are based on organic semiconductors - carbon-based materials whose backbones are comprised mainly of alternating C–C and C=C bonds [4]. In 1959, Kallmann and Pope reported the first attempt to fabricate OPV devices where they studied the photovoltaic response of a structure that contained a single crystal of anthracene sandwiched between two electrodes [5]. It was from then that a few attempts followed this adventure. The study area however became of interest to many people especially in the past two decades as witnessed by the ever increasing number of publications in the area [6].

1.2.1 Why Organic Solar Cells

There are several reasons pointing to why organic solar cells deserve their place in the sun. Overally, the sun is a primer and an environmentally safe source of energy for our globe. Conventional silicon solar cells as opposed to organic solar cells still suffer from being expensive, non-flexible hence less suitable for roll-to-roll mass production and some specific uses, toxic to the environment and require high temperatures for production. Organic solar cells have gained much attention over the past two decades [6] with their current power conversion efficiency reaching around 15% [6-8]. This is because of their promised characteristics which include lightweight, flexibility [6], cheapness and suitability for rapid processability through roll to roll printing methods [9] among others.

Among various solar technologies, organic photovoltaic technology distinguishes itself as an economically feasible solution owing to its mass production capability by means of low-cost roll-to-roll manufacturing although the high cost of raw materials, like functionalized fullerenes, often seems counter. Furthermore, mechanical flexibility, light weight, and transparency of OPV enable portable, wearable energy sources or window tinting applications which cannot be realized by inorganic photovoltaic technology [6].

From these various promising researches done on organic solar cells, and the ever-improving power conversion efficiency, it is clear that the future of organic solar cells will yield better results and improved functionalities.

1.3. OPV Materials and Devices

Mostly, OPVs in the laboratory scale are usually fabricated on rigid substrates, epitomized by glass, for inexpensive and facile processing [6]. Generally, an organic solar cell consists of a glass substrate, active layer, positive and negative electrode, hole and electron transport layer. According to layer structure, organic solar cells are grouped into two groups namely the conventional and the inverted layer structure [4, 6]. It is mainly the arrangement of the hole transport layer (HTL) and the electron transport layer (ETL) that differentiates the two. This can be seen in Figure 1.1 below which shows the conventional and the inverted layer structure of organic solar cells.

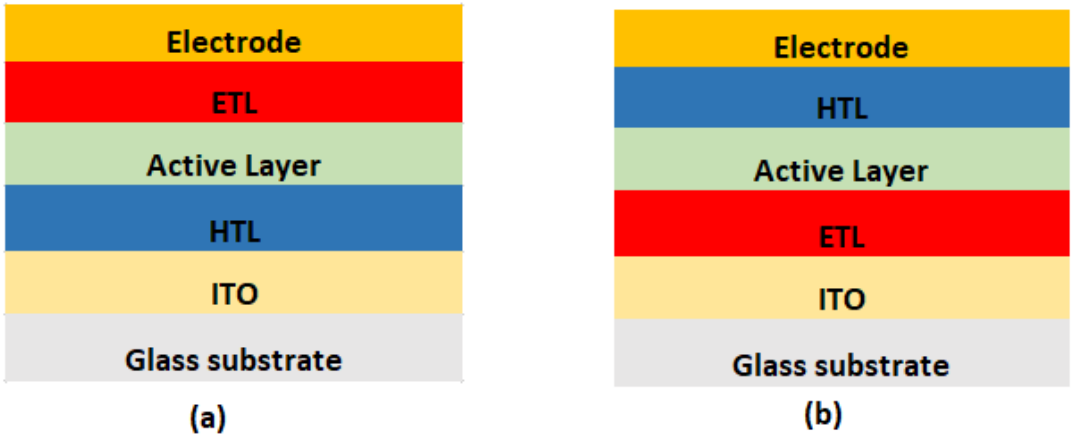

Figure 1.2 Conventional (a) and Inverted (b) layer structure of organic solar cells

As can be seen in Figure 1.2 above, an organic solar cell consists of different layers of materials with different properties. Hence the need to study and characterize the respective layers.

1.3.1. Glass substrate

This is the first layer on which all the other layers are laid on. It is the thickest of all the layer as its thickness is usually in the range of a millimeter. Glass substrates maintain planarity during processing and ease of handling of the device [6]. In terms of light interaction, glass substrate layer plays an important part because of its millimeter size and

the fact that it is located on the side of the incident light. Examples of glass substrates used in organic solar cells include quartz glass, microscope glass and indium tin oxide (ITO) coated glass, calcium fluoride glass and silicon dioxide glass. For commercial OPVs, flexible substrates are used. Almost all of these glass substrates have high transmission in the visible range. In ITO coated glass substrates, the usual effect of the glass substrate is the reduction of reflection, since the refractive index of glass is less than ITO [10].

1.3.2. Photoactive layer

An organic solar cell photoactive layer is basically sandwiched between the hole transport and the electron transport layer in most cases between an indium tin oxide (ITO) covered substrate (glass or plastic) and a reflective aluminum back electrode. The charge carrier extraction is driven by internal electric fields across the photoactive layer caused by the different work function electrodes for holes and electrons [4]. It is in this layer that the absorption of light happens and hence the need to study the optical properties of all layers in front and those that comes after the photoactive layer to ensure maximum absorption in the photoactive layer. Usually the layers that are in front of the photoactive layer (to the glass side) have more transmission and those that are after the photoactive layer are reflective to ensure no light leaves the organic solar cell multilayer.

Some examples of photoactive layers used for organic solar cells include P3HT:PCBM (Poly(3-hexylthiophene):[6,6]-phenyl-C61-butyric acid methyl ester) and PBDB-T:ITIC where P3HT and PBDB-T are donor polymers while PCBM and ITIC are fullerene and no-fullerene acceptors respectively. Full name for the polymer PBDB-T is poly[(2,6-(4,8-bis(5-(2-ethylhexyl)thiophen-2-yl)-benzo[1,2-b:4,5-b’]dithiophene))-alt-(5,5-(1’,3’-di-2-thienyl-5’,7’-bis(2-ethylhexyl)benzo[1’,2’-c:4’,5’-c’]dithiophene-4,8-dione)] and full name for the non-fullerene acceptor ITIC is 3,9-bis(2-methylene-(3-(1,1-dicyanomethylene)-indanone))-5,5,11,11-tetrakis(4-hexylphenyl)-dithieno[2,3-d:2’,3’-d’]-s-indaceno[1,2-b:5,6-b’]dithiophene.

The photoactive layer is made of conducting materials. Conducting organic materials can be classified either as donors, which readily lose electrons, or as acceptors, which readily accept electrons. The main challenge for photoactive layer is to enhance light

absorption while maintaining limited thickness for efficient charge transport. Hence the need to optically model and simulate the organic solar cell multilayer in order to determine the optimal photoactive layer thickness. The route to all this has to pass through determination of optical constants of organic solar cell materials.

1.3.3. Hole Transport Layer (HTL)

This is the part of the solar cell that transport holes to the electrode. Poly(3,4-ethylenedioxythiophene) polystyrene sulfonate (PEDOT:PSS) has been dominantly used as a hole transport layer (HTL) in OPVs and its function is to block electrons and transfer holes to the electrode [10]. It has a high work function of about 5.0 eV and thereby effectively reduces the hole injection barrier [6]. PEDOT:PSS also planarizes the rough surface of ITO and therefore prevents any local short circuiting. Other HTL materials for organic solar cells include MoO_3 for inverted organic solar cells.

1.3.4. Electron Transport Layer (ETL)

Examples of hole transport layer are the PCBM in P3HT:PCBM solar cells and ZnO in inverted organic solar cells. PCBM, which is a soluble derivative of buckminsterfullerene, remains the most popular electron transporter in polymer solar cells [6].

1.3.5. Electrodes

Once the charge carriers have been successfully separated, they need to be transported to the respective electrodes to provide an external direct current. Common examples of electrodes include ITO and metals such as Ag and Al. ITO has been the most dominant transparent conducting positive electrode in OPVs to collect generated holes, owing to its good transparency and conductivity [6, 10]. It is chosen because of its transparency since it is placed in the front of the solar cell layer system. Metal electrodes include aluminium and silver and they act as cathodes capturing electrons.

Some examples of electrodes include the polyethylenimine (PEI) which has been widely used to produce low-work-function electrodes [11]. PEI is of low cost compare to other electrodes and is environmentally friendly.

Figure 1.3 below summarizes the layer structure and interaction of HTL, ETL, ITO, photoactive layer and glass substrate in an organic solar cell [4]. The use of lithium fluoride as an underlayer for aluminium electrode improves the charge injection.

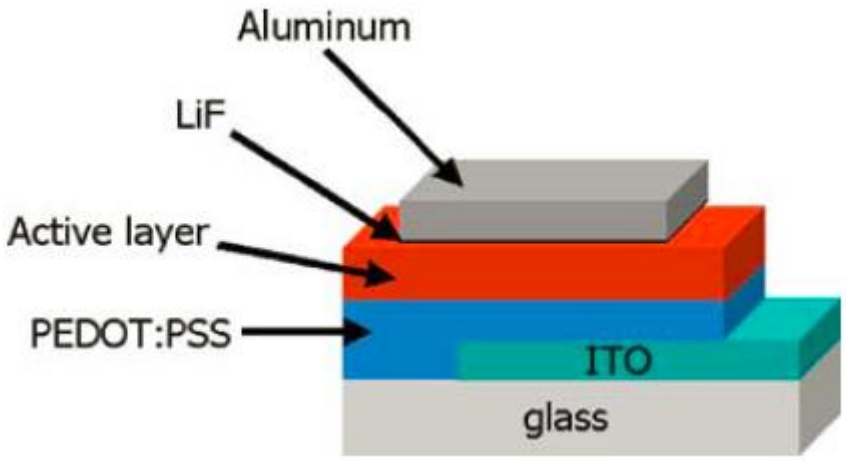

Figure 1.3 Schematic design of an organic solar cell. The photoactive layer is sandwiched between optimized electron (Al) and hole extracting (ITO) electrodes [4].

1.4. Introduction to Optics and Optical Constants

Optics of organic solar cells involves light interaction with matter and to understand this a prior knowledge of the general properties of light is needed. The sub sections below will describe both the general properties of light and properties of light interaction with matter.

1.4.1. Properties of Light

Light has both wave and particle nature. This is termed wave-particle duality of light where light has both wave and quantum particle properties. Figure 1.4 below shows the wave particle duality of light.

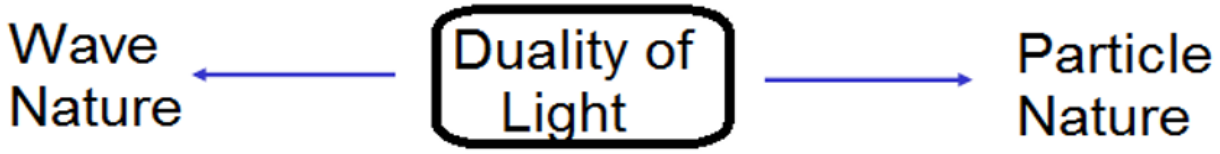

Figure 1.4 Wave particle duality of light

1.4.1.1. Wave nature of light

The wave nature of light can be proved with diffraction and interference. Light can travel through a vacuum and follows the general wave equation. Equation

c =$f\lambda$ (1) below shows the general wave equation which light waves also satisfies.

$$c = f\lambda \quad (1)$$

where c is velocity, λ is the wavelength of the light wave(s). For a vacuum $c=f\lambda$ where c =3.0x10^8 m/s. Thus the wave nature views light as a continuous wave. As a transverse electromagnetic wave, light has its electric or magnetic field vibrating in time and space. Below is the wave equation for an electric field waveform propagating in vacuum [12].

$$\nabla^2 E - \mu_0 \epsilon_0 \frac{\partial^2 E}{\partial t^2} = 0 \quad (2)$$

The solution to this equation will be:

$$E(r,t) = E_0 Cos(k \cdot r - \omega t + \emptyset) \quad (3)$$

where ∅ represents an arbitrary (constant) phase term. The vector k can be written as:

$$k = \frac{2\pi}{\lambda} \hat{u} \quad (4)$$

where λ is vacuum wavelength, û is the unit vector defining the direction of propagation. λ is also the length by which r must vary to cause the cosine to go through a complete cycle [13].

1.4.1.2. Particle nature of light

Particle nature of light views light as a quantized energy source. Generally, light is absorbed and emitted in tiny discrete bursts, in "particles" of electromagnetic quantities known as photons. A photon is a packet of light energy. Each photon has an energy E given by:

$$E = hv \quad (5)$$

where h is Planck's constant, v is frequency. Photoelectric Effect proves the particle nature of light [12]. Photoelectric effect is the emission of electrons (photo electrons) when light shines on a material. Polarization effects are a result of the wave interaction of light with the physical world. Light is a transverse electromagnetic wave made up of mutually

perpendicular, fluctuating electric (E) and magnetic field (B). Figure 1.5 below shows the orientation of B and E [13].

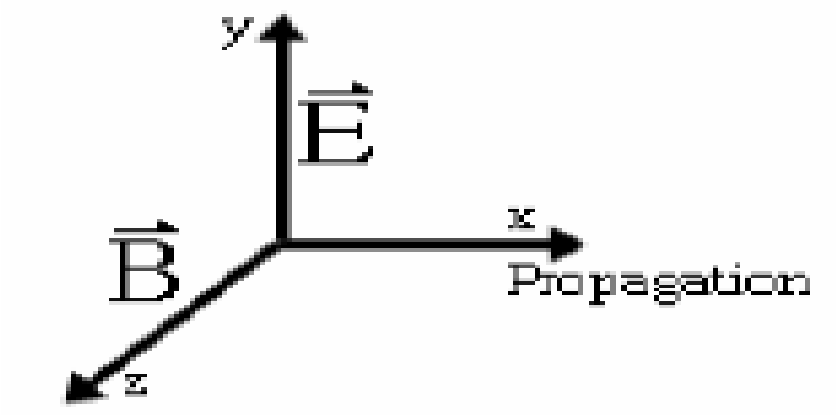

Figure 1.5 Orientation of electric field E and magnet field B

1.4.2. Light interactions with matter

Light can interact with matter through three processes namely transmission, absorption and reflection. Solar radiation striking a surface will either be reflected, absorbed, or transmitted. The combination of these three phenomena will equal 100%. Reflection (%Reflectance) is an interface, or surface phenomenon while Transmission (%Transmittance) is a bulk phenomenon. For opaque materials, solar radiation will not transmit, it will only be absorbed or reflected. Reflectance is the ratio of reflected light to incident light and it refers specifically to the visible portion of the solar electromagnetic radiation spectrum. Figure 1.6 below illustrates transmission, reflection and absorption.

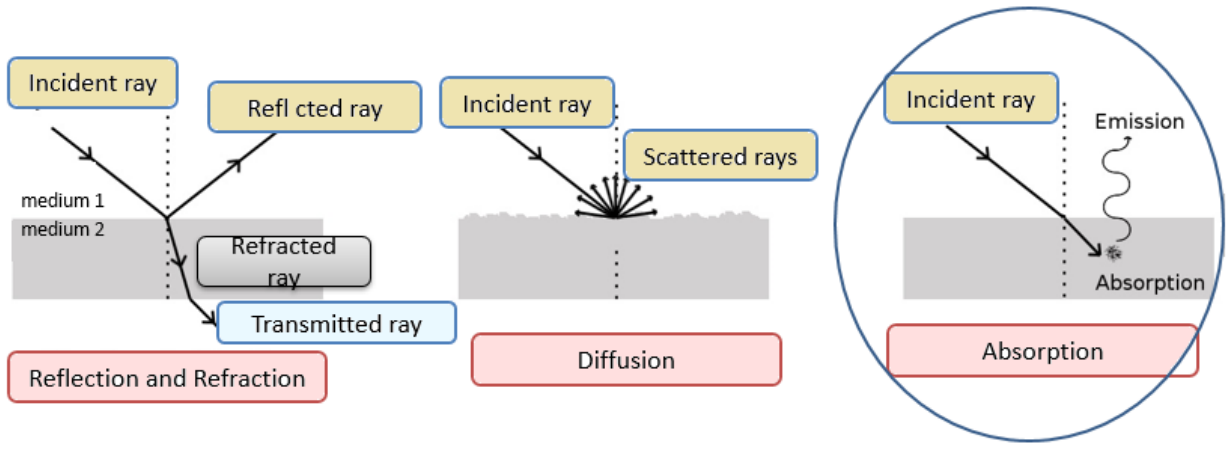

Figure 1.6 Diagramatic illustration of transmission, reflection and absorption.

1.4.2.1. Absorption

Absorption A is given by the equation below.

$$A=1-(T+R) \qquad (6)$$

where T is transmission and R is Reflection. For absorption the energy of the "swallowed" photon is transformed into the excitation energy of a cloud of electrons. This energy can be converted into vibrational energy of the material or into several energetically weaker infrared photons. Absorption of light strongly depends on its specific wavelength. For any multilayer system, backward transmission T' = forward transmission T, but backward reflection R' = forward reflection R only for a non-absorbing layer system for which backward absorption A' = forward absorption A and is equal to zero. The absorption of light by an optical medium is quantified by its absorption coefficient (α), which is defined as the fraction of absorbed power in a unit length of medium. Absorption coefficient α is given by:

$$\alpha = 4\Pi k/\lambda \qquad (7)$$

where λ is wavelength [14].

Interaction of light with matter involves the absorption of a photon by an atom or a molecule. If the photon has the required energy, the atom or molecule will be raised from a low energy state to one of higher energy. After a short period of time the atom or molecule falls back to a lower state and the energy difference is emitted as a photon. Figure 1.7 below shows the absorption process.

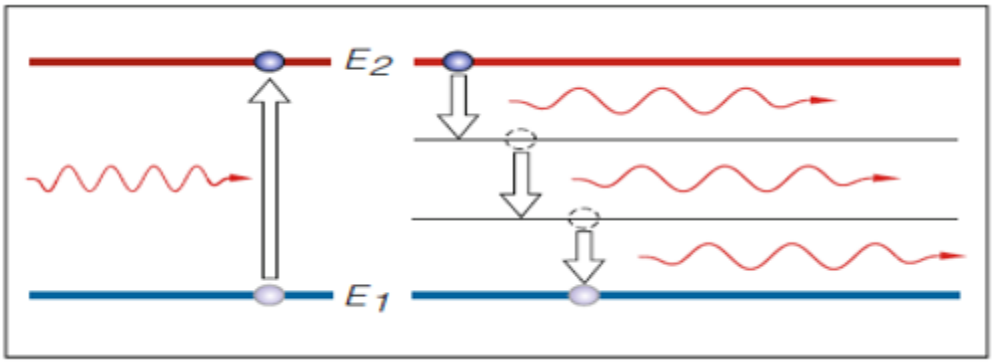

Figure 1.7 Absorption of a photon and dispersion of energy into lattice vibrations. The absorbed light energy warms the absorber [15].

Different materials have different absorption profiles. Figure 1.8 below shows typical absorption coefficients of water, melanin, collagen and haemoglobin.

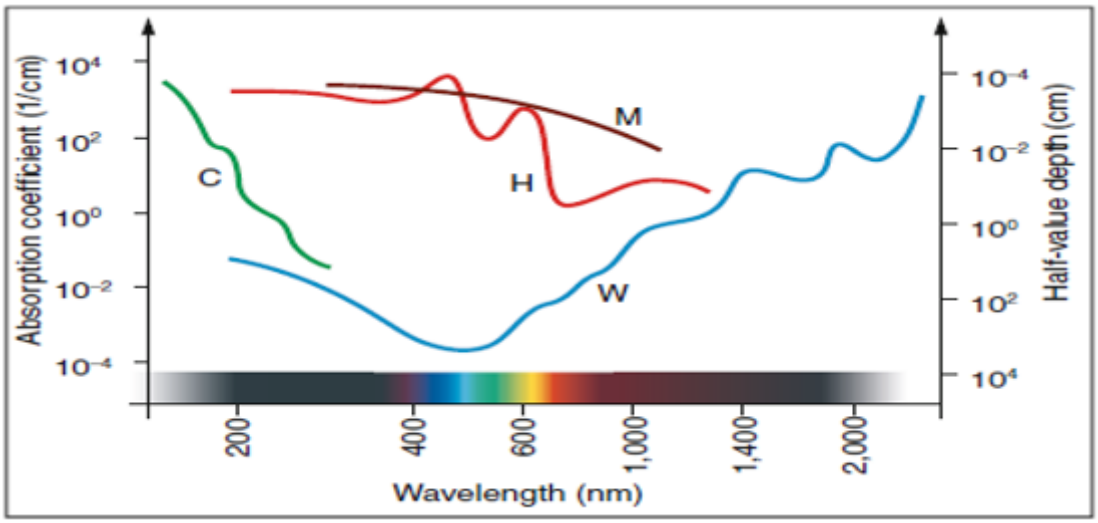

Figure 1.8 Absorption coefficients of Water W, Haemoglobin H (in physiological concentration of 150g/l), Melanin M, and collagen C. Left coordinate is in units of cm^{-1}. For right coordinate half is absorbed by the time it has reached this far. Water is very transparent in the visual range and strongly absorbing in the infrared range [15].

1.4.3. Reflection, Refraction and Refractive Index

When a beam of light strikes an interface of two different media, some light is scattered backward some is refracted into the forward medium as it is transmitted. Refraction is when an incident light ray is bent or when travelling from one medium to the other. Incident light ray and the reflected ray are always in the same plane. In the case of transmission, the scattered wavelets cancel each other in the forward direction [12]. Figure 1.9 below shows a plane of incidence to illustrate incident ray of light, refracted and reflected light.

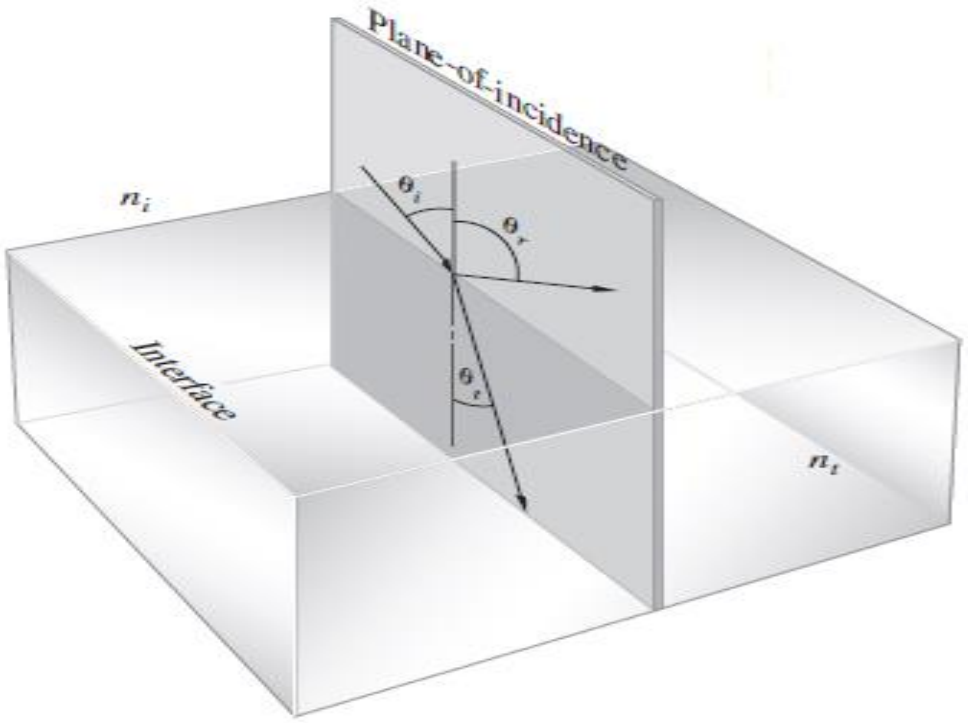

Figure 1.9 Illustration of a plane of incidence together with the incident ray of light, refracted and reflected light ray. θ_i is angle of incidence, θ_t is angle of refraction [12].

The real part (n) of the complex refractive index is a dimensionless physical quantity, which is specific for a certain medium. Its value characterizes the speed of light in a medium and it depends on the wavelength of incident light. Absolute n is defined as a ratio of the speed of light in vacuum and in selected medium. Relative n is defined as a ratio of speeds of light in two different media

Whenever light impacts the interface between two media (1 and 2), it is partially reflected and partially refracted. This is described by Snell's law:

$$n_{12} = \frac{Sin\alpha}{Sin\beta} = \frac{v_1}{v_2} = \frac{n_2}{n_1} \qquad (8)$$

where α is incident angle, β is angle of refraction, v_1 and v_2 are the speeds of light in medium 1 and 2 respectively [16]. Different refractive indices between media leads to reflection. Law of reflection states that: angle of incidence = angle of reflection. Refractive index n can also be defined as the ratio of speed of light in vacuum (c) in to that in the medium (v):

$$n = c/v \qquad (9)$$

For example n(glass)=1.520, n(water)=1.333, n(air)=1.000

Optical density is the degree to which a refractive medium retards transmitted rays of light. Optical density of any transparent medium is a measure of its real refractive index n. A medium with a relatively high n is said to have a high optical density [17]. The higher the refractive index the higher the reflective losses for a medium. Thus, transparent medium usually has close to one refractive index. When light is refracted into the optically sparser medium and the incident angle is greater than the critical angle, all light is reflected. Metals have a high real and imaginary refractive index values [17].

The optical path represents the distance light travels in a vacuum in the same time it travels a distance d in the medium. Optical path (Δ) $nd=ct$ where c is speed of light in a vacuum and t is time in seconds.

If a light ray travels through a series of optical media of thickness d, d', d'', ... and refractive indices n, n', n'', ... The total optical path is the sum of the separate optical paths. Figure 1.10 shows an illustration of optical path length.

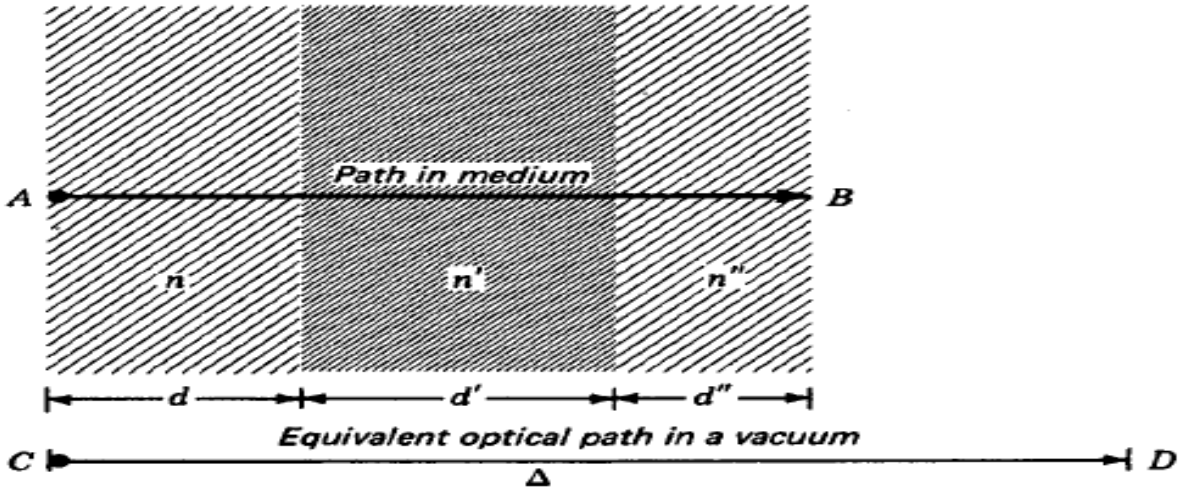

Figure 1.10 Optical path length of a material [17].

1.4.4. Complex Dielectric Function

A dielectric material is a material whose negatively charged particles are strongly bound to some positively charged nearby particles. Its negatively charged particles are not free to move. Examples of dielectrics include ceramics, polymers, thin films, and rubber. Applying an external electric field to a dielectric material will make charged particles to

move only slightly away from their normal position. The movement of the charges against restraining molecular forces provides the material with the ability to store electric energy. The parameter used to represent the relative (compared to free-space) charge storage capability of a dielectric material is the dielectric constant or relative permittivity ε_r.

The absolute permittivity of a material "ε", referred to as the dielectric function/constant is given by:

$$\varepsilon = \varepsilon_r \varepsilon_0 \qquad (10)$$

where ε_0 is permittivity of free space, ε is usually referred to as dielectric function and is a measure of the polarizability of a material. It is the capability of a material to separate charges inside its body. By definition, dielectric constant of a vacuum is 1. Metals are the most polarizable materials in nature, so their dielectric constant is the highest.

Dielectric constant depends on frequency of applied electric field, chemical structure, temperature and pressure of material [18]. Most common techniques for determining the dielectric function of a material involve measuring its reflection coefficient, transmission coefficient, and refractive index.

For a multilayer system, each layer is defined by its complex index of refraction ñ where

$$\tilde{n} = n + ik \qquad (11)$$

where k is the extinction coefficient. Extinction coefficient is a measure of how strongly a substance absorbs light at a given wavelength. It is related to the absorption coefficient α which is the fraction of the power absorbed in a unit length of the medium and given by:

$$\alpha = \frac{4\Pi k}{\lambda} \qquad (12)$$

where λ is wavelength.

The complex index ñ takes account of absorption as well as the usual oscillatory behaviour of the light wave [14]. The complex dielectric function ε is directly related to ñ where

$$\varepsilon = \tilde{n}^2 \qquad (13)$$

Thus, when a time-harmonic electric field is applied to a dielectric material, the relative permittivity of the medium is recognized to be complex and given by:

$$\varepsilon = \varepsilon' - j\,\varepsilon'' \qquad (14)$$

where ε′ is the real part and ε″ is the imaginary part. The real part ε′ describes the polarizability of the material under test. The imaginary part ε″ stands for dielectric losses according to the phase-shifted movement of polar molecules in an electromagnetic field [14].

1.4.4.1. The Lorentz Model of Dielectrics

The Lorentz model of dielectrics describes the dielectric polarization at microscopic level. Assuming that all atoms (or molecules) in dielectric medium are identical, and each atom has one (or a few) active electrons responding to the external field, then:

$$Polarization\ P = q_e N r_{micro} \qquad (15)$$

N is number of identical active electrons per volume uniformly distributed in space, r_{micro} is a microscopic displacement of the electron from equilibrium. Thus in a dielectric material, each dipole has strength $q_e r_{micro}$ [13].

1.4.4.2. Polarization

When a dielectric is subjected to an applied electric field, the internal charge distribution is distorted. This corresponds to the generation of electric dipole moments, which in turn contribute to the total internal field. The external field then separates positive and negative charges in the medium (each pair of which is a dipole). These charges then contribute an additional field component. The resultant dipole moment per unit volume is called the electric polarization P [12]. P is a measure of the difference between the electric fields with and without the medium in place.

$$(\varepsilon - \varepsilon_0)\boldsymbol{E} = \boldsymbol{P} \qquad (16)$$

where **E** is electric field.

1.4.4.3. Snell's law

When unpolarized light is incident on a dielectric medium such as a glass, the reflected rays are partially plane-polarized. Light is a mixture of a plane polarized and unpolarized (ordinary) light. Considering a plane light wave striking a boundary between two media having refractive indexes n_1 and n_2. If the angles φ, φ' and φ'' are the angles

of incidence, reflection, and refraction, respectively then, $|\varphi| = |\varphi'|$, law of reflection. The Snell's law of refraction is given by:

$$n_1 sin\ \varphi = n_2 sin\ \varphi'' \qquad (17)$$

At a certain angle of incidence φ_B, the reflected light is totally plane – polarized. This angle is called the "Brewster's Angle" or "Polarizing Angle", and it is related to the refractive index of the medium by the Brewster angle shown in Equation 18 below [19].

$$\frac{n_2}{n_1} = tan\ \varphi_B \qquad (18)$$

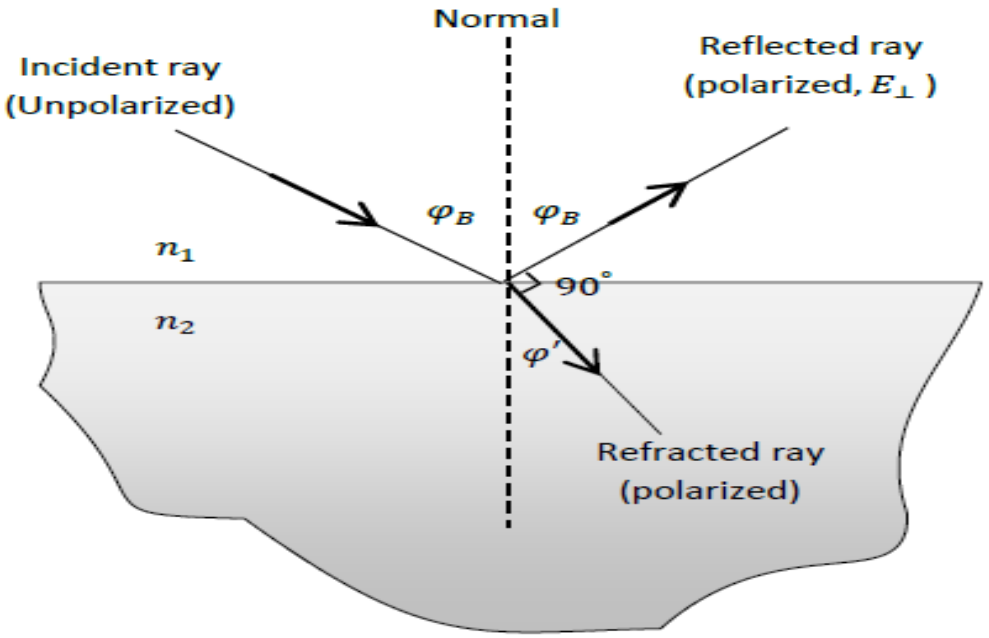

Figure 1.11 Brewster's angle representation.

At Brewster's angle, the reflected beam is completely polarized and the refracted beam is perpendicular to the reflected beam. For the Brewster's angle, the reflected electric vector E is normal to the plane of incidence. It is an angle of incidence at which light with a particular polarization is perfectly transmitted through a transparent dielectric surface, with no reflection[19].

Optical setups are often oriented such that a laser beam propagating through them is at Brewster's angle. That way, reflection losses are avoided for p-polarized light without requiring any anti-reflection coatings. Figure 1.12 shows the s and p polarization in light waves.

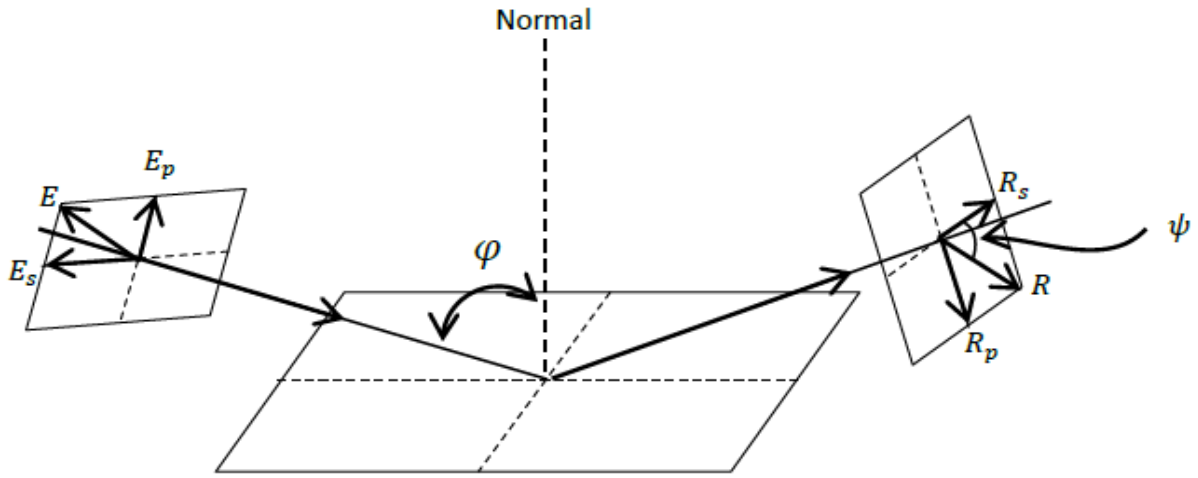

Figure 1.12 Light polarization [19].

1.4.5. Fresnel Equations

Fresnel equations describe the reflection of light at an interface based on the index of refraction of the two materials at the interface, the angle of incidence, and the polarization of the light with respect to the plane of incidence [12, 19]. For light moving from one medium to the other, the vector E in the incident, reflected or refracted light can be resolved into two amplitude components:

- p – components - E_p, R_p and E'_p that are parallel to the plane of incidence
- s – components - E_s, R_s and E'_s that are normal to the plane of incidence

For unpolarized light, $E_p = E_s$. Fresnel equations basically describe the reflection and transmission of electromagnetic waves at an interface. They give the reflection and transmission coefficients for p and s waves. The refracted wave always retains the phase of the incident wave. For the components of the reflected wave (Rp and Rs), the phase relations depend on n_1 and n_2.

Rather than measuring the amplitude, it is usually convenient to measure the intensity of the light wave, that is its energy flux carried. The intensity is proportional to the square of the amplitude. The ratios of the average energy fluxes over a period of time in the reflected and refracted waves to the average energy flux in the incident wave are called the reflection coefficient *r* and the transmission coefficient *t*. The Fresnel equations

that define the reflection and transmission coefficients for the s- and p-components of the incident wave now becomes:

$$r_s = \left(\frac{R_s}{E_s}\right)^2 \quad (19)$$

$$r_p = \left(\frac{R_p}{E_p}\right)^2 \quad (20)$$

$$t_s = \left(\frac{E_s'}{E_s}\right)^2 \quad (21)$$

$$t_p = \left(\frac{E_p'}{E_p}\right)^2 \quad (22)$$

In the absence of light absorption,

$$r_s + t_s = 1 \quad (23)$$

and

$$r_p + t_p = 1 \quad (24)$$

in accordance with the law of the conservation of energy [12, 19].

1.4.6. Interference, Coherent and Incoherent Light Propagation

Light is a series of propagating electric field E and magnetic field B oscillations. Interference occurs when two or more light waves pass through the same region and add to or subtract from each other. Diffraction occurs when light waves pass through small openings or around small obstacles and spread [15]. Polarization occurs due to the transverse nature of the electric field vibration in a propagating electromagnetic wave [19]. Interference and diffraction result by applying the wave superposition as a propagation principle of light through the system.

Constructive and destructive interference of light waves is also the reason why thin films, such as soap bubbles, show colorful patterns. Optical properties of thin films are mostly due to interference effects of more than two waves. The millimeter sized glass substrates used in organic solar cells bring interference due to incoherent light propagation in that layer [10, 20].

1.5. Literature on Optical Characterization and Modelling of Organic Solar Cells Materials

Optical characterization and modelling of films and solar cells involves using experimental data for the films to characterize and model each organic solar cell film (layer material). The process usually involves determination of optical constants of each organic solar cell layer and simulation of the whole organic solar cell multilayer to determine optimum parameter. Optical constants consist of the complex refractive index made up of the real (n) and the imaginary part (k).

1.5.1. Methods used in Literature for Obtaining Optical Constants of Organic Solar Cell Materials

Various research has been carried out in the characterization of organic solar cells and their respective materials. Table 1 below shows methods used for obtaining optical constants of organic solar cell materials.

Table 1 Methods used for obtaining optical constants.

Method	Short Description	References
Ellipsometry	Ellipsometry is a non-destructive, fast and accurate characterization technique used for determining the thickness and the optical constants of a material. The data is interpreted more based on the modelling than the experimental data.	[21]
Kramers-Kronig Relations (KKR)	KKR are bidirectional mathematical relations, connecting the real and imaginary parts of any complex function.	[22, 23]
Exponential decay (Beer-Lambert law) method	This method assumes optical intensity follows the exponential decay as light will be propagating in organic solar cell layers. Following this exponential decay, optical constants can be estimated for each layer. Song et al [24], compared the transfer matrix method to the exponential decay from which slight differences were observed.	[24]
Modelling dielectric functions	Uses software such as Scout/CODE to determine optical constants of organic solar cell materials through fitting dielectric functions to measured R and T measurements of each layer. The method is usually accompanied by the transfer matrix formalism to model the whole organic solar cell multilayer system.	[25, 26]
Rigorous Coupled Wave Analysis (RCWA) method	Uses partially coherent sources. Alaibakhsh and Darvish proved that RCWA produces a smoother absorption spectrum when compared to using coherent sources. However, the change in the absorption efficiency witnessed was negligible.	[10]
Determination of optical constants from IV and EQE measurements	Enables extraction of complex refractive index from the external quantum efficiency (EQE) and current–voltage measurements. Lenze et al successfully obtained optical constants from EQE and IV measurements.	[27]

There are however other ways of determining optical constants that use averaging or algorithmic approaches. These include the Bruggeman's effective medium approach [28] for determining optical constants of two phase material from the optical constants of the constituent materials. This is usually integrated in optical modelling platforms.

QiYing, et al [29], came up with a modified algorithm method for the determination of optical constants and film thickness of blended organic thin film. A simple and convenient method was established to calculate optical constants of two-phase material using the blending of copper phthalocyanine (CuPc) and fullerene (C60) layer films.

1.5.2. Technologies and Methods used in Optical Characterization and Modelling of films and organic solar cells

The work of this thesis is also linked to processes such as interference, coherent and incoherent light propagation and the transfer matrix formalism [30]. There are various techniques linked to optical characterization and modelling of organic solar cell materials. While the techniques used might slightly differ, the backbone of the standard procedure such as determination of n and k values and then use the same values to simulate the whole organic solar cell multilayer system are almost followed in many of the researches done.

Harbecke, in 1985 came up with an accurate method to model coherent and incoherent reflection and transmission of multilayer structures using the transfer matrix method [20]. The method eliminated the usually difficult to eliminate Fabry-Perot resonances which rise due to the glass substrate being several times thicker than other layers. Interference within this thick film was suppressed by adding the absolute squares of the partial waves corresponding to an incoherent treatment. It is against this background of transfer matrix formalism that this thesis follows especially for the simulation of an organic solar cell multilayer system.

Song et al [24], studied the optical interference effect in layered organic materials in which calcium fluoride was used as the glass substrate. From the results, there was qualitative and quantitative similarity between the transfer matrix calculation used and experimental results indicated that optical intensity in these organic films can be modulated based on their thicknesses.

Monestier et al [31], modelled organic solar cells based on CuPc and C60. From the results prediction of short-circuit current Jsc of single planar heterojunction organic solar cells was made.

This work will be based on the procedure taken by Hoppe et al [26] on the determination of optical constants. The thesis however involves use of CODE software in the determination of optical constants instead of the younger version SCOUT. After determination of optical constants, the so-called transfer matrix formalism was used to simulate the organic solar cell multilayer system taking into account the interference effect. Key objectives will be to determine optical constants of common materials used in organic solar cell and use them to simulate an organic solar cell multilayer system in order to obtain optimized parameters or theoretical limits.

1.6. Motivation for Optical Characterization and Modelling of OPVs

Recently, the highest efficiency records for organic photovoltaics have moved into the range of 10-15% for various types of materials [6, 7]. Such impressive efficiencies were obtained after several years of analysing the behaviour of these materials and optimizing the fabrication procedures. Optical properties are one of the contributing factors to obtaining highly performing organic solar cells.

Optical modelling and simulation are therefore important tools that can be used to understand the light behaviour in organic solar cell multilayer system. Optical modelling can be used to identify key design features of the organic solar cell device, and to identify areas of poor performance. Thickness of all layers in an organic solar cell can be optimized to achieve highest internal absorption based on the agreement between optical models and measurement data. Optical modelling is important to separate the parasitic absorption (absorption in non-active layers) which does not contribute to photocurrent generation, and the photons absorbed by the active layer alone, which should be counted when determining the overall power conversion efficiency of an organic solar cell.

Optics of organic solar cells is all about light interaction with a multi-layer system. Since an organic solar cell consists of a layer stack of different materials it is of primordial importance to study and understand the optical properties of each layer in order to understand how light propagates through the multilayer system. In this thesis optical constants of organic solar cell materials will be obtained with the aim of simulating the whole organic solar cell multilayer system.

Optical constants consist of the complex refractive index which is made up of the real part and the imaginary part. Optical properties play an important part in understanding light interaction with organic solar cell multilayer system. Optical constants n and k can be used to fully describe the reflection, transmission, the phase shift and the absorption of respective layers [13]. Furthermore, it is from the same n and k values that some important parameters such as the current density, external quantum efficiency (EQE) and internal quantum efficiencies can be extracted.

In most cases for one to perform optical modelling there is need of experimental data for the characterization (reflection and transmission) of the respective material. It is from the same n and k values that the simulation of an organic solar cell multilayer system is done. Therefore, just the optical constants (n and k) only can be used to successfully describe an organic material in order to determine needed parameters. Furthermore, an understanding of optical constants will bring an easier understanding of other properties of organic solar cell materials such as electrical properties. Furthermore, the maximum current that the solar cell can deliver strongly depends on the optical properties of the solar cell, such as absorption in the absorber layer and reflection.

As time moves, new materials for organic solar cells are being discovered. Examples of these new materials include the use of non-fullerene acceptors to obtain better power conversion efficiencies in OPVs [8, 32, 33]. However, in order to obtain the maximum performance from these new materials, there is need to study their optical behavior which can best be done through obtaining their optical constants from which all other studies will be done. In line with this, optical modelling and simulation will act as an initial cheaper optimization in order to determine desired parameters. Hence the need for optical characterization, modelling and simulation of organic solar cell materials.

The layers in an OPV device are thin (nm range) such that they generate interference effects with each other [34]. Due to this, it is therefore difficult to directly measure the incident light absorption in the active layer without the influence of the other device layers in the multilayer OPV stack. However, optical modelling is a useful approach to quantify

the internal absorption of photoactive layers in the device taking into account interference effects.

1.7. Research Plan

This thesis is based on an optical characterization and modelling of organic solar cell layers. To achieve this various stages and processes will be carried out. Organic films and solar cells were prepared and characterized followed by modelling of dielectric functions of each layer film to determine the optical constants for each film. Finally, the whole organic solar cell layer(s) will be simulated to determine the amount of light absorbed in the active layer. From om this simulation, variation of active layer thickness with current density will be determine together with the maximum number of photons generated for each thickness. The Bruggeman's effective medium approach was also used to approximate the optical constants of two phase active layer material from the optical constants of its constituent materials. Figure 1.13 below shows the flowchart presenting both the goals of this thesis and their implementation procedure.

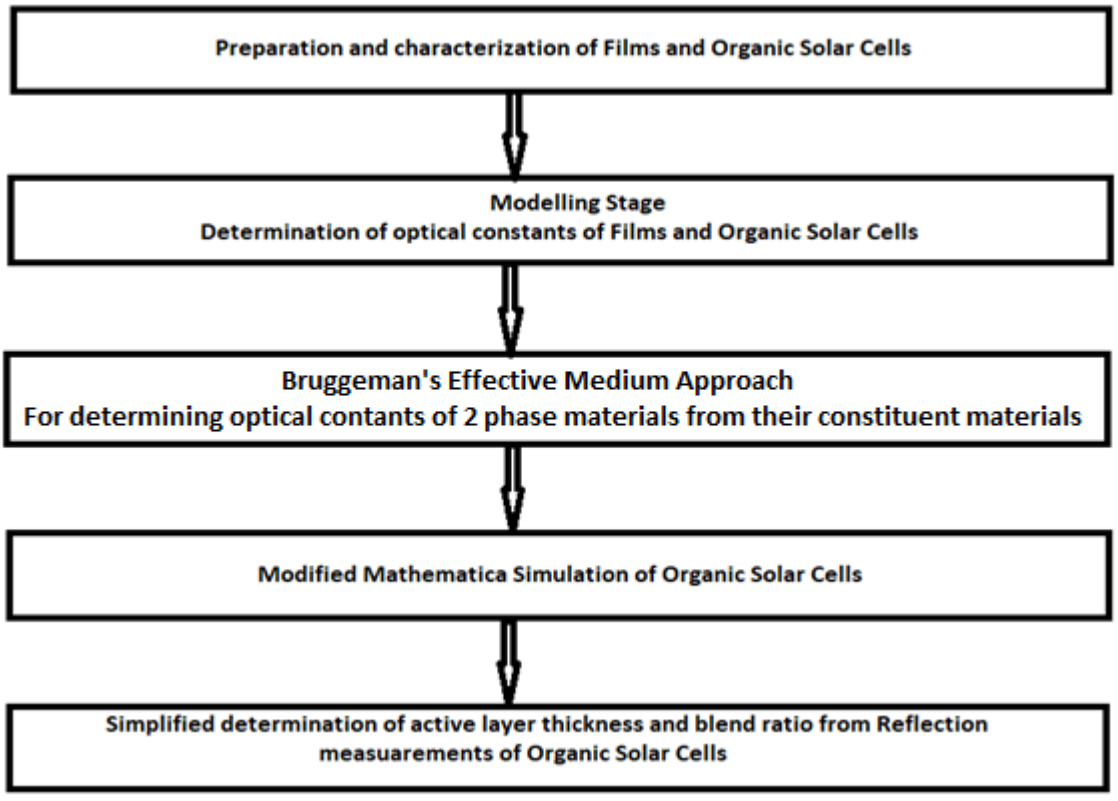

Figure 1.13 Flowchart of the Research Plan

To enable a clear sub structuring of ideas for the sake of understanding, this thesis is divided into seven (7) Chapters with Chapter 2 giving the full experimental details and procedures taken to prepare and characterize films and organic solar cells. Chapter 3 gives the computational approach which aims to describe the development of the used models and simulations. Apart from outlining the theory and physics of the optical modelling approach, this Section also covers the optical modelling of a specified multilayer OPV system. In Chapter 4, results of this work and the respective discussions are presented portraying both the findings and the extracted meanings. Finally, the conclusions of this work and a suggestion for future avenues of research based upon these findings are presented in Chapter 5.

2. EXPERIMENTAL DETAILS

This Section summaries all the measurements techniques and procedures that were employed in the optical characterization and modelling of films and organic solar cells. Background information critical to the application of the measurement techniques will be outlined, and the specific experimental details used for each technique will be explained. This Chapter will serve as a general reference for all of the techniques commonly employed across the various parts of this thesis thus preventing repetition of identical material in future chapters. Wherever any of these techniques are altered or further adapted for a particular theme of study within the thesis, the adaption will be specifically described in detail in the relevant Chapter.

2.1. Materials

Materials used for this thesis include substrates, chemicals and solvents. This Section aims to describe fully the materials used for making films and organic solar cells for optical characterization, modelling and simulation.

2.1.1. Chemicals

This sub-section describes the chemicals and solvents used in this thesis. A donor material poly[(2,6-(4,8-bis(5-(2-ethylhexyl)thiophen-2-yl)-benzo[1,2-b:4,5-b']dithiophene))-alt-(5,5-(1',3'-di-2-thienyl-5',7'-bis(2-ethylhexyl)benzo[1',2'-c:4',5'-c']dithiophene-4,8-dione)] (PBDB-T) and a non-fullerene acceptor 3,9-bis(2-methylene-(3-(1,1-dicyanomethylene)-indanone))-5,5,11,11-tetrakis(4-hexylphenyl)-dithieno[2,3-d:2',3'-d']-s-indaceno[1,2-b:5,6-b']dithiophene (ITIC) was purchased from California Organic Semiconductors Inc (Cal-OS). Poly(3,4-ethylene- dioxythiophene):(polystyrene sulfonic acid) (PEDOT:PSS) was purchased from Heraeus Clevios GmbH (Germany). PBDB-T was purchased from Cal-OS, USA while ITIC was obtained from Institute for Organic Chemistry and Makromolecular Chemistry (IOMC), Jena, Germany.

Toluene and chlorobenzene solvents were purchased from Sigma Aldrich (USA) for all device fabrication purposes. 99% methanol was obtained from Alfa Aesar GmbH & Co. UV-curing barrier epoxy resin (LP 651, Delo Industrial Adhesives, Germany) was used to encapsulate OPV devices after fabrication. Films were prepared by spin coating from

chlorobenzene solutions of 1:1 (by weight) blends of PBDB-T and ITIC as used in the standard organic solar cells. PEDOT:PPS was spin cast from an aqueous solution with a concentration of 0.5% by weight. 99 % methanol was used to wash away the PSS part of the PEDOT:PSS at the same conditions as that of PEDOT:PSS.

2.1.2. Substrates

All substrates were cleaned with isopropanol in an ultrasonic bath previous to spin coating the layer films. In order to determine the optical constants of both layers of the ITO glass, the transparent ITO was first etched away completely using concentrated HCl and Zinc powder to allow for the determination of optical properties of the substrate glass alone. The complete ITO glass was also measured.

Different glass substrates were used in this work for the sake of characterization comparisons. Substrates used include quartz glass, microscope glass slides and etched Indium-doped tin oxide (ITO) glass (ITO glass without ITO) and ITO glass (with ITO). Quartz glass of thickness 1.5mm was purchased from GVB GmbH (Germany). Glass microscope slides of thickness 1 mm were purchased from Thermo Scientific. ITO coated glass (Rs = 15 Ω/sq) of thickness 1.1 mm was purchased pre-patterned from Xin Yan Technology Ltd (Hong Kong, China) and used directly as an OPV electrode.

Quartz glass substrate was used for all films while ITO glass substrate was used for solar cells. Quartz glass substrate was chosen because of its better transmission in ultra violet (UV) region compared to other glass substrates. Figure below shows all the glass substrates used in this work.

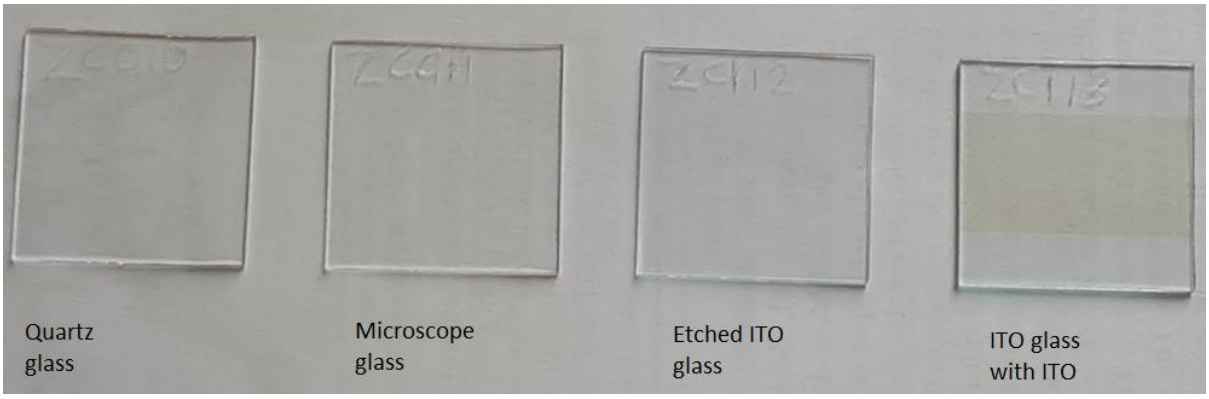

Figure 2.1 Glass substrates used for optical characterization and modelling

2.2. Films preparation

Films prepared were grouped into three groups namely substrates, metals and oxides and active layer materials. A film is basically a layer material on a substrate. The substrates used in organic solar cells are usually glass substrate as described in the substrates sub-section above. PEDOT:PSS was placed in the group of metals and oxides group while glued microscope was in the substrates group.

2.2.1. Metals and metal oxide layers

Al, MoO3, Mg and Ag were prepared by vapour deposition in a glove box. TiOx was prepared inhouse where 15% TiOx was mixed with isopropanol. The solution was spin coated and annealed at 80 °C in air. A drop while method was used to drop the TiOx on a quartz glass substrate while spin coating. The layers Al, Ag and Mg/Ag are used in organic solar cells as electrodes. Normally common material for electrodes is a metal with a thickness of more than 100 nm such that no transmission will happen through. Table 2 below shows the metal and metal oxide films prepared with the respective conditions as shown.

Table 2 Metals and metal oxide films

Substrate type	Layer 1	Layer 2	Spin Frequency (rpm)	Annealing Conditions	Thickness (nm)
Quartz glass	PEDOT:PSS		3000	180 °C, 10 minutes	40
Quartz glass	ZnO		5000	170 °C, 10 minutes	35
Quartz glass	PEI		2500	105 °C, 10 minutes	50
Quartz glass	Al				70
Quartz glass	MoO3				12.5
Quartz glass	Ag				200
Quartz glass	Mg	Ag			240
Quartz glass	TiOx		2500	80 °C, 10 minutes	30
ITO glass with ITO	PEDOT:PSS			180 °C, 10 minutes	180
ITO glass with ITO	ZnO		5000	170 °C, 10 minutes	175

2.2.2. Active Layer material films

The concentration of PBDB-T:ITIC used was 7.5 µg/ml with 99.5% chlorobenzene as a solvent. Vaniline (0.5%) was used as an additive. Volume ratio of 1:1 was used for PBDB-T:ITIC. Both the substrates and active layer solutions were kept at 80 °C before spin coating on which 60µl was used for spin coating. Active layer films of PBDB-T, ITIC and PBDB-T were spin coated on quartz glass substrate in a glove box.

Table 3 below shows the active layer films prepared and the conditions for the preparation.

Table 3 Active layer material films

Substrate	Layer 1	Layer 2	Layer 3	Spin Frequency (rpm)	Thickness (nm)
Quartz glass	PBDB-T			2500, drop while	40
Quartz glass	ITIC			2500, drop while	60
Quartz glass	PBDB-T:ITIC			2500, drop while	80
Quartz glass	PEDOT:PSS	PBDB-T:ITIC			120
ITO glass w.o. ITO	ITO	PEDOT:PSS	PBDB-T:ITIC		260
ITO glass w.o. ITO	ITO	ZnO	PBDB-T:ITIC		255

2.3. Optical characterization of films and organic solar cells

Reflection, transmission and photoluminescence measurements were measured using an Avantes Spectrometer for all the films.

2.3.1. Avantes UV-, VIS-, NIR- Spectrometers

Near-normal incidence (7°) transmission and reflection spectra of the spin cast films on all substrates were recorded using the Avantes Avaspec spectrophotometers in the range between 250 and 1050 nm. The Avantes spectrometers can measure in the ultra violet, visible region and near infrared light region. Figure 2.2 below shows a setup of the Avantes Avaspec spectrophotometers used to measure the reflection, transmission and photoluminescence of the films.

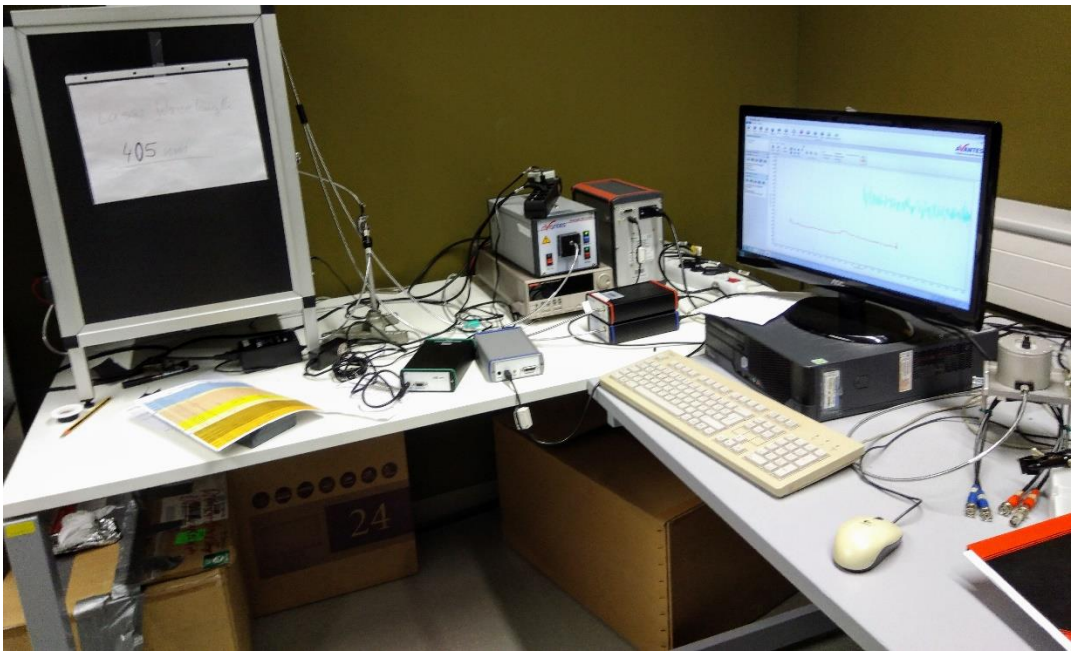

Figure 2.2 Avantes avaspec spectrometers for measuring Reflection, Transmission and Photoluminescence.

Layers involved in the organic solar cell stack were optically characterised. Films consisting of PBDB-T, ITIC, PBDB-T:ITIC, ZnO, MoO_3, PEI, Al, ITO, PEDOT:PSS, TiOx were deposited on a quartz glass substrate in order to fully characterize them. For all the films, Reflection and Transmission were measured. For the films consisting of the active layer materials (PBDB-T, ITIC and PBDB-T:ITIC), reflection, transmission, photoluminescence were measured. Thicknesses of all prepared films were measured using Atomic Force Microscopy (AFM).

2.3.2. Solar Cells Preparation

Solar cells with the layer structure Glass/ITO/PEDOT:PSS/PBDB-T:ITIC/Mg/Al were prepared. The materials and procedure for the preparation of the solar cells is as described in Chapter 2 above. For the solar cells, IV and EQE measurements were done. Figure 2.3 below shows the schematic layer structure of the solar cells prepared. Results of the solar cells prepared are as shown in Chapter 4 below.

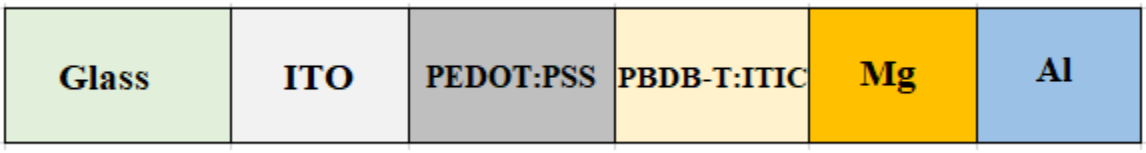

Figure 2.3 Layer structure of the organic solar cell.

3. COMPUTATIONAL APPROACH

This Section gives the computational methods involved in modelling and simulation of films organic solar cells. Results from optical characterization (R and T measurements) were used for modelling stage and results of the modelling stage (n and k values) will be used for simulation.

3.1. Optical Modelling

Optical constants of films and organic solar cell layer stacks were determined by fitting model dielectric functions to reflection and transmission spectra of the respective layers using CODE software. Results of the optical modelling will be complex refractive indices (n and k), complex dielectric functions. Depending on the need, absorption coefficient can also be obtained from the modelling. To make sure the imported measured data of R and T fits the model(s), different susceptibilities have to be used to match the material being modelled.

3.1.1. Complex Model Dielectric Functions

These are models that help describe the dielectric response of a material. Dielectric models, sometimes referred to as susceptibilities used for this thesis include the following:

3.1.1.1. Dielectric Background

This is the simplest dielectric model that can be applied to a material. It is used where there is a constant background and the imaginary component of the dielectric function is zero. This oscillator has been used to describe low absorbance materials such as the glass substrate used in OPV devices. In most cases the real part of the dielectric function will be equal or close to zero.

3.1.1.2. Drude Model

This is used in the case of materials with free charge carriers such as doped semiconductors and metals. Free charge carriers in semiconductors and metals have very important contributions to the dielectric function. The charge carriers set free by the donors or acceptors can be accelerated by very little energies and hence do respond to applied electric fields with frequencies in the infrared region [35].

3.1.1.3. Kim Oscillator

This is an extension of the simple harmonic oscillator model for vibrational modes suggested by Kim et al [36] in 1992. A Kim oscillator is an extension of the simple harmonic oscillator model for vibrational modes and it allows a continuous shift of the line shape between a Gaussian and a Lorentzian profile [35]. It is a flexible oscillator that is useful to describe the optical transitions that may be occurring in semiconductor materials.

3.1.1.4. Lorentz Oscillator

In an insulator, the electrons are tightly connected with the nucleus of the atoms. Any external influence on the system, such as an electric field, leads to a generation of an opposite dipole by the electron. This interaction was described by Lorentz for insulators, non-doped and doped semiconductors [35].

3.1.1.5. Brendel Oscillator

This is an improved version of a simple harmonic oscillator model. It accounts for local variations in disordered systems by a Gauss distribution of resonance frequencies [35].

3.1.2. Fitting complex dielectric functions

Optical constants of films and organic solar cell layer stacks will be determined by fitting model dielectric functions to reflection and transmission spectra of all layers in the solar cell device using CODE software. Fitting parameters are those parameters that are changed in order to optimize the agreement of the model. Both the dielectric function and the refractive index are called optical constants. The fitting of complex model dielectric functions to the transmission and reflection spectra as well as the determination of the active layer thickness and blend ratio from reflection measurements of a complete solar cell was performed using the software. The model dielectric functions consist of a constant dielectric background contributing to the real part of the dielectric function, and oscillators to describe the respective materials. Figure 3.1 below shows the susceptibilities that were used to obtain the n and k values of microscope glass.

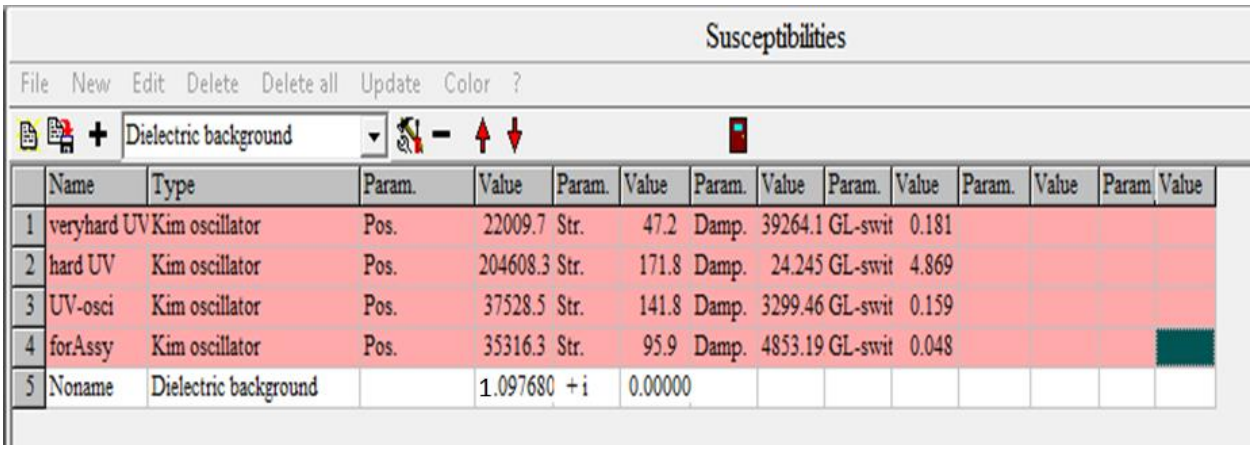

	Name	Type	Param.	Value	Param.	Value	Param.	Value	Param.	Value	Param.	Value	Param	Value
1	veryhard UV	Kim oscillator	Pos.	22009.7	Str.	47.2	Damp.	39264.1	GL-swit	0.181				
2	hard UV	Kim oscillator	Pos.	204608.3	Str.	171.8	Damp.	24.245	GL-swit	4.869				
3	UV-osci	Kim oscillator	Pos.	37528.5	Str.	141.8	Damp.	3299.46	GL-swit	0.159				
4	forAssy	Kim oscillator	Pos.	35316.3	Str.	95.9	Damp.	4853.19	GL-swit	0.048				
5	Noname	Dielectric background		1.097680	+i	0.00000								

Figure 3.1 Susceptibilities used for modelling microscope glass.

3.1.2.1. Steps in Developing a Model from Reflection and Transmission Measurements

The following are the steps followed when developing a model in CODE software using reflection and transmission experimental data.

- Define materials in the Materials Section of the CODE tree view and define the range of the data
- Input the layer stack in the tree view layer stack Section. Drag and drop the materials from Materials into the respective layers in the Layer stack
- Import Reflection and Transmission measurements data into the respective A,T,R spaces in Simulated Spectra
- Input the susceptibilities of the materials in the layer stack
- Define fitting parameters in the Fitting Parameters tree view Section
- Keep on working on susceptibilities and fitting parameters until the model for R and T fits the measured data.
- Export required output data and/or graphs which can be optical constants (n and k values), complex dielectric functions, energy loss or absorption coefficient.

3.1.3. Effective Medium Approach (EMA)

Effective Medium Approach is a method that enables mixing of optical constants and through its special averaging techniques the optical constants of a composite material can be determined from the optical constants of its constituent materials. This is sometimes

generally referred to as mixing of optical constants for heterogeneous materials (two-phase composites) [35]. Various effective medium approach techniques exist which include the so-called Bruggeman approach, the classical Maxwell Garnett approach, the Looyenga formula and the Bergman representation [35, 37]. Of these, the Bruggeman and Maxwell Garnett effective medium approaches are the most prominent ones. In 1935, Bruggeman developed a method [28] that can be used to determine optical constants of inhomogeneous materials. The method has been used successfully in different materials [37-40] to determine optical constants.

In this thesis, Bruggeman effective medium approach is used to determine the optical constants of the active layer blend. From the optical constants of pristine PBDB-T and ITIC, optical constants of PBDB-T:ITIC blend were determined. Figure 3.2 below shows the input section of the composite materials to be used for Bruggeman method and the Bruggeman equation as used in CODE software. Results of the Bruggeman method and the results of fitting dielectric functions to the experimental reflection and transmission measurements were also compared and a conclusion drawn as shown in the results Section.

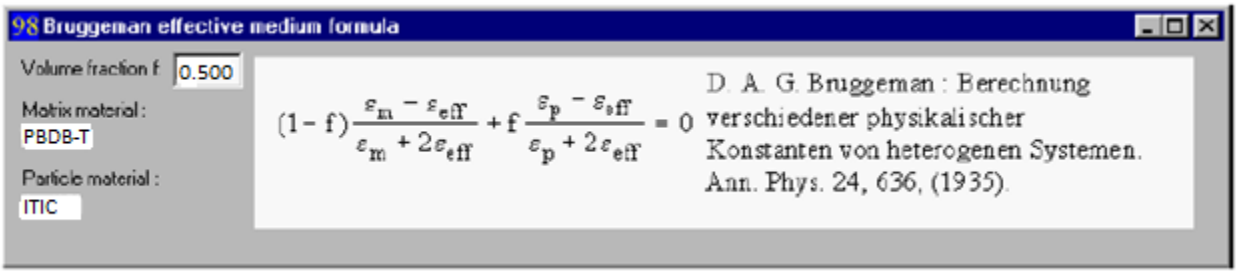

Figure 3.2 Input section of the Bruggeman approximation and the Bruggeman equation.

3.2. Simulation of Organic Solar Cell Multilayer System.

In order to simulate the organic solar cell multilayer system, the so-called transfer matrix formalism (TMF) is used [20, 25, 30]. Transfer Matrix Formalism is an efficient method of modelling a multilayer system in which the multilayer is treated as a one-dimensional system. Each layer is described by its complex reflective index, ñ = n + ik, and the incident light will reflect at each interface layer and transmit through each layer medium.

Due to interface reflection, TMF considers two electromagnetic waves, one propagating in positive direction $E^{+}{}_{m}$ (x) (forward propagated wave) perpendicular to the interfaces of the multilayer system, and one in the opposite direction $E^{-}{}_{m}$(x) (backward propagated wave). By traveling from layer A to layer B, the wave undergoes Fresnel reflection and transmission [12, 25]. Figure 3.3 below shows an organic solar cell layer structure used showing the forward and the backward propagation electromagnetic waves. The illustration of the multilayer system shown was done following what has been done in [25]. Since the electric field E is related to the magnetic field B, the transfer matrix formalism considers variation of electric field in the multilayer system.

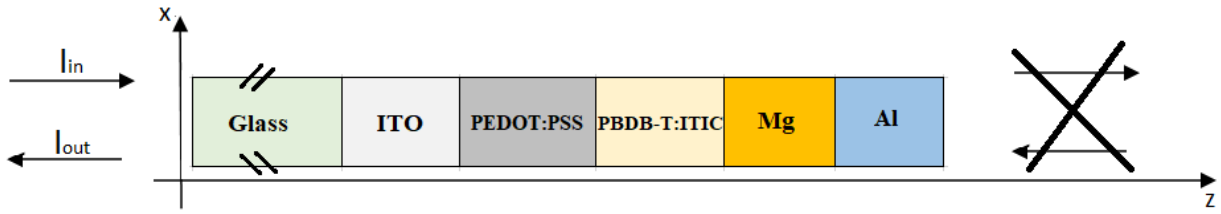

Figure 3.3 Layer structure of the organic solar cell showing the forward and backward propagation matrices.

The continuity equation for the energy (given below) describes the amplitude and phase of the system at any arbitrary point.

$$Q + div\bar{S} = 0 \qquad (25)$$

$$\bar{S} = c^2\varepsilon_0 \boldsymbol{E}x\boldsymbol{B} \qquad (26)$$

Q denotes the local time averaged absorption while the Poynting vector $\bar{S}$ denotes the denotes the electromagnetic energy flux density which is power per unit area crossing a surface [12, 19, 25]. The program for simulating the organic solar cell multilayer was written using ‘‘Mathematica’’ (WOLFRAM Research, Champaign, IL, USA) and treats the case of normal incidence of the light by use of transfer matrix formalism. The procedure followed was as done in [20, 25] where the whole organic solar cell multilayer was treated as a one dimensional system. As can be seen light approaches the organic solar cell from the glass side. In addition, the layers of an organic material are assumed to be homogeneous and isotropic [20]. Since the thickness of the glass substrate (mm range) is way larger than the coherent wavelength of light (about 800 nm), there is incoherent light propagation in

the glass substrates. Hence the need for a method such as the transfer matrix formalism used in this work which takes into account the incoherent propagation in the millimeter sized glass substrate.

Light enters the multilayer through the glass substrate and sequentially passes through ITO, PEDOT:PSS, PBDB-T:ITIC active layer and then it is reflected by the aluminium electrode. Due to the high reflectivity and absorption of the aluminum electrode, no light leaves or enters from the right side of the device. The reflected light leaves the solar cell again at the glass front. The simulation results are as shown in Chapter 4 below.

4. RESULTS AND DISCUSSION

This Section gives the results and a brief discussion of the results of the optical characterization and modelling of films and organic solar cells.

4.1. Results for Preparation and Characterization of Films and Organic Solar Cells

This sub section gives the results of the preparation and characterization of films and organic solar cells.

4.1.1. Substrates

Thickness of glass substrates was measured using a micrometer screw gauge with an accuracy of +/- 0.01 mm. Since ITO is a thin layer in range of nanometers there was no reasonable difference between the thickness of ITO glass with ITO and ITO glass without ITO when measured using a micrometer screw gauge. The thicknesses of the glass substrates are as shown in Table 4 below.

Table 4 Thickness of glass substrates used.

Substrate Type	Thickness (mm) +/- 0.01 mm
Quartz glass	1.13
Microscope glass	1.02
Etched ITO glass	1.10
ITO glass with ITO	1.10

Figure 4.1 below shows the transmission results for all substrates compared together with air. As can be seen from the results quartz glass has the highest transmission in UV, visible and near infrared region. This is the same reason why all the films were prepared on quartz glass.

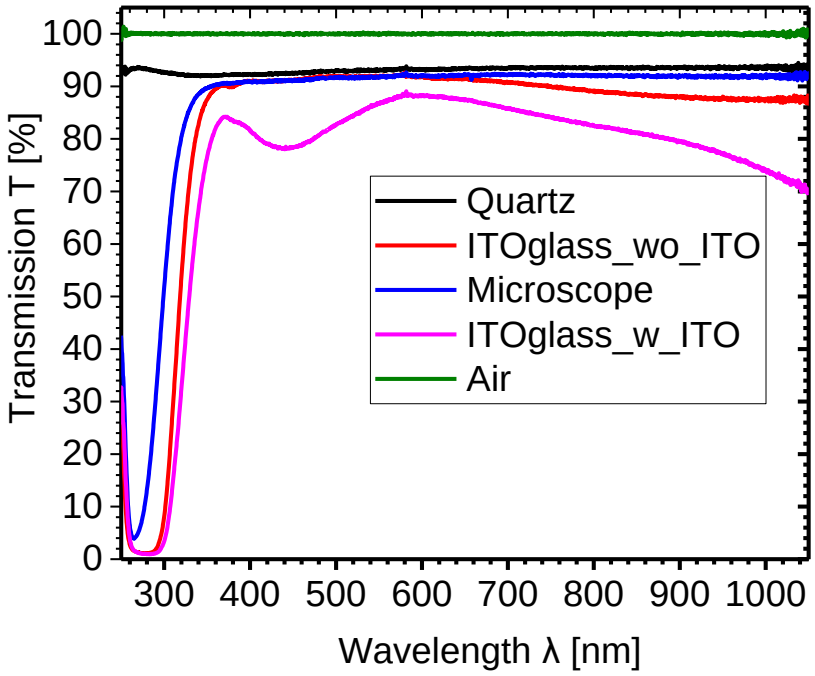

Figure 4.1 Transmission results for all substrates. ITOglass_w_ITO and ITOglass_wo_ITO represent ITO glass coated with ITO and ITO glass without ITO (etched ITO glass) respectively.

4.1.2. Reflection and Transmission Results for metal and metal oxide films

4.1.2.1. Metal Electrodes Comparison

Figure 4.2 below shows R and T comparison for different metal films that are commonly used as electrodes for organic solar cells. For these electrode materials, there should be close to zero transmission as this will be the last layer of the organic solar cell. Therefore, the reflection and absorption of the electrodes should be as high as possible for the not to be light escaping the organic solar cell multilayer system.

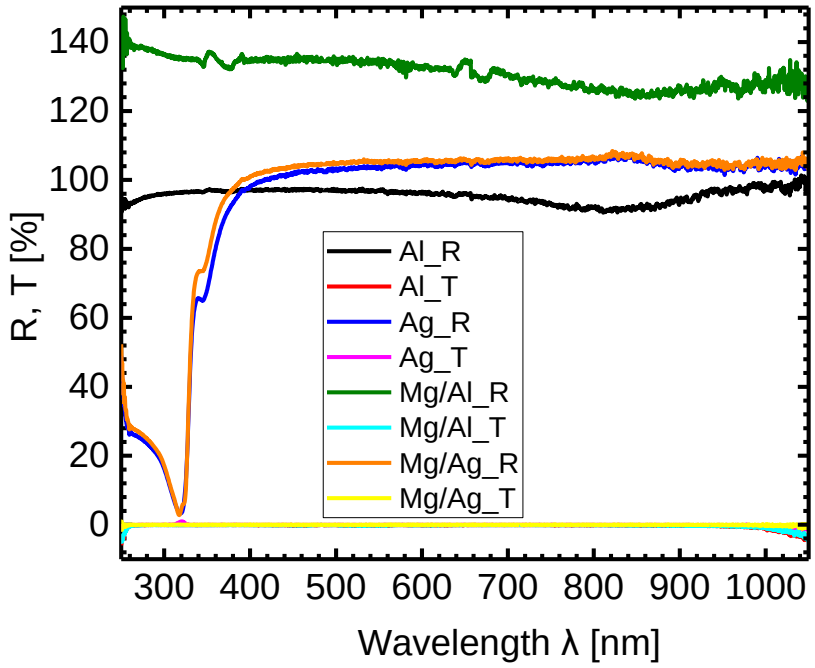

Figure 4.2 Reflection and Transmission results for Ag, Al and MgAl films.

From Figure 4.2 above it can be seen that Al has a higher Reflection in the ultra violet region than Ag and Mg/Ag and a slightly lower reflection in the visible and near infrared region. As can be seen from the Figure, all of the films have zero transmission which is what is required in order not to have light passing through. Mg/Al layer has the highest reflection and in this case it appears to be more than 100% (which should not be the case) because of the calibration of Al sample which was used for the spectrometer. However the normal Reflection of the mg/Al layer should be near 100%.

4.1.2.2. Results for All Other Metal and Metal Oxide Films

Figure 4.3 below shows R, T and A plot for Quartz/ZnO film.

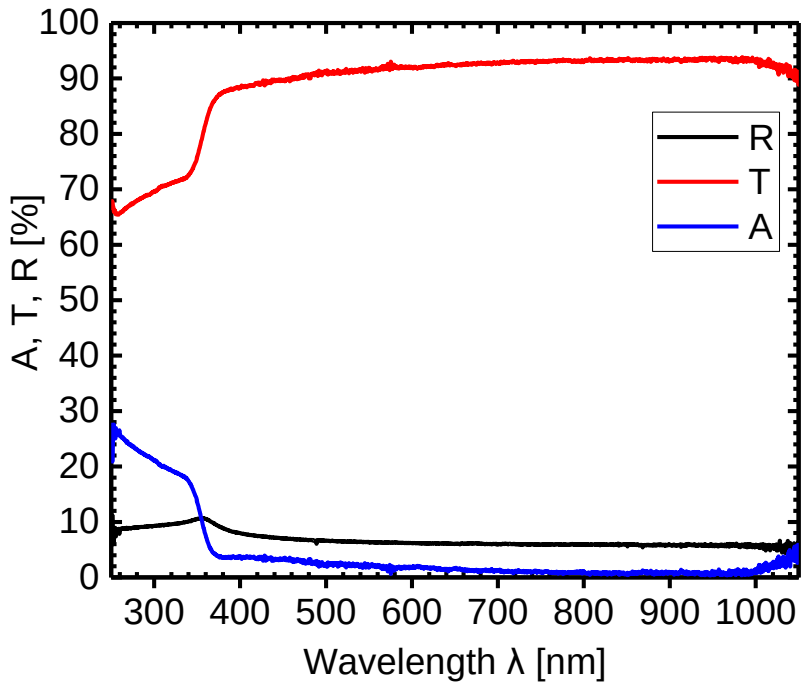

Figure 4.3 Quartz/ZnO film R, T and A plot.

ZnO has a lower absorption and higher transmission in the visible region.

Figure 4.4 Quartz/PEDOT:PSS film R, T and A plot.

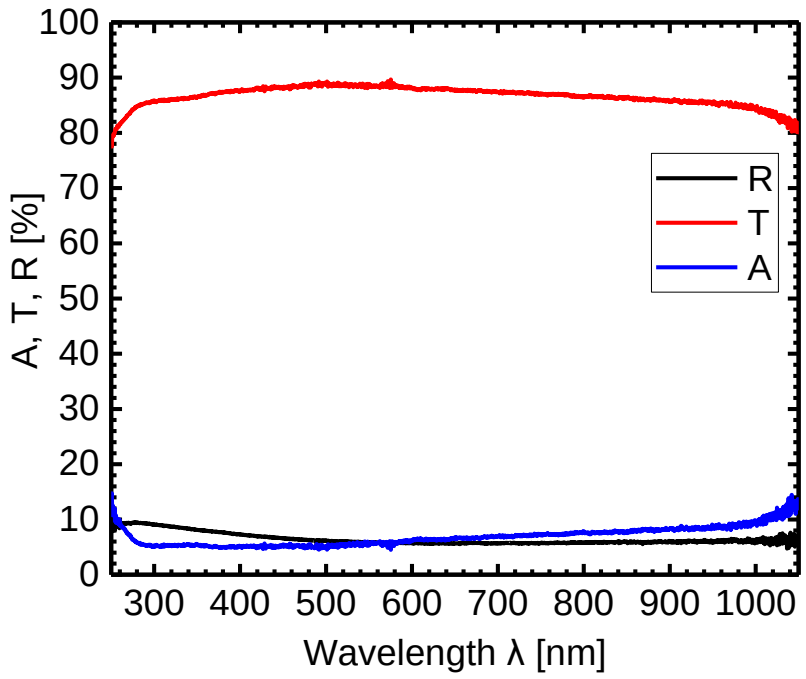

Figure 4.4 Quartz/PEDOT:PSS film R, T and A plot.

Figure 4.5 Quartz/MoO_3 film R, T and A plot.

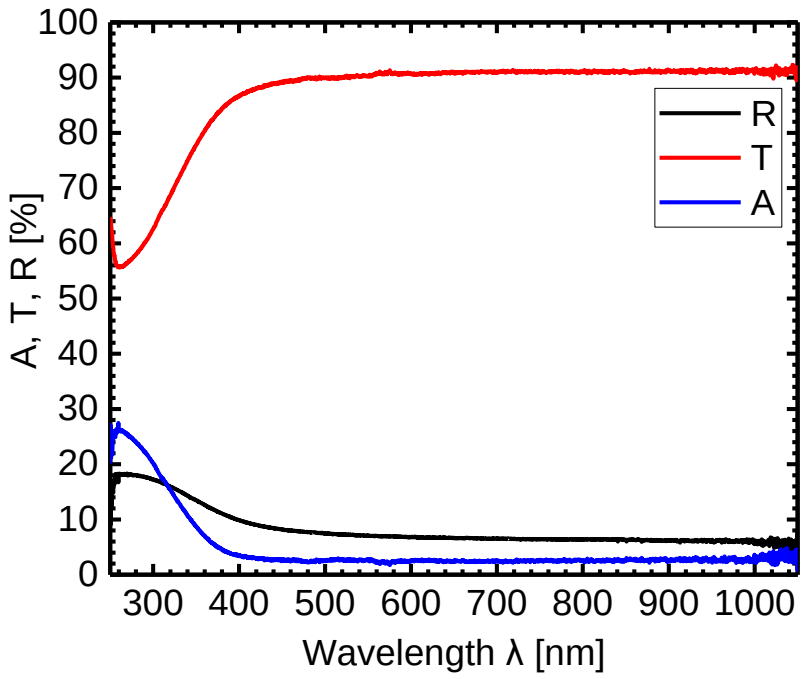

Figure 4.5 Quartz/MoO_3 film R, T and A plot.

Quartz/TiOx

Three spin frequencies were used for the film Quartz/TiOx which are 700 rpm, 1000rpm and 2500 rpm. This was to vary the thickness of the TiOx films and observe the variation of the reflection, transmission and absorption of the films. Figure 4.6 below shows the plot for Quartz/TiOx films with different spin frequencies.

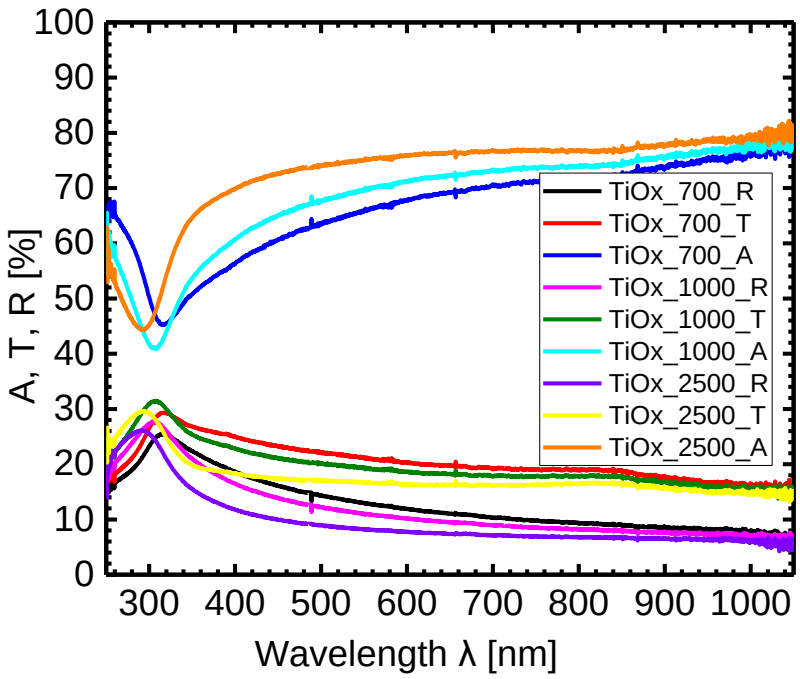

Figure 4.6 R, T and A plot for Quartz/TiOx films with different spin frequencies.

Quartz/PEI

Figure 4.7 below shows Quartz/PEI films of different thicknesses. Three spin frequencies were used to vary the thicknesses which are 700 rpm, 1000rpm and 2500 rpm. It can be seen that the thinner the film, the more transmission it has.

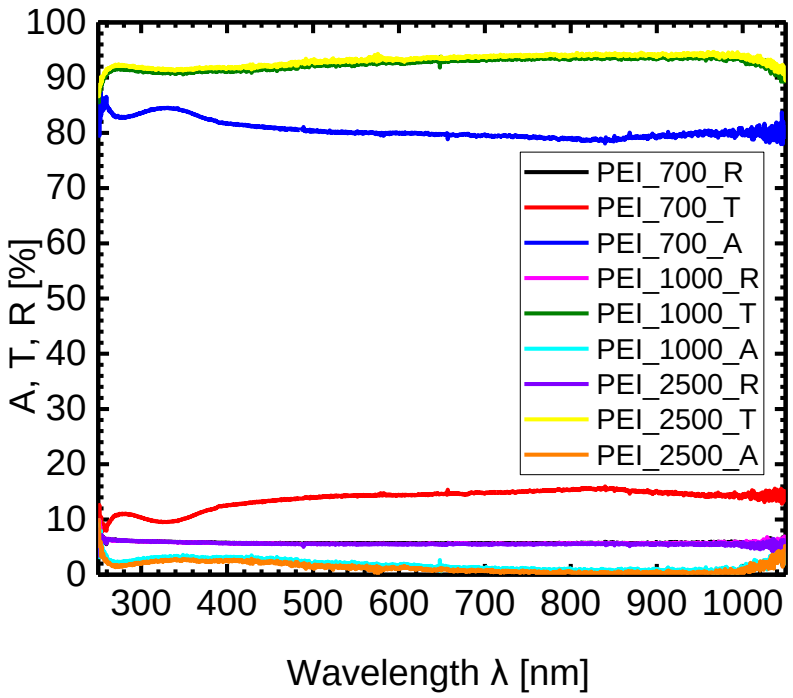

Figure 4.7 R, T and A plot for Quartz/PEI films with different thicknesses.

ITO glass/ITO/PEDOT:PSS

Figure 4.8 below shows R, T and A plot for ITO glass/ITO/PEDOT:PSS film.

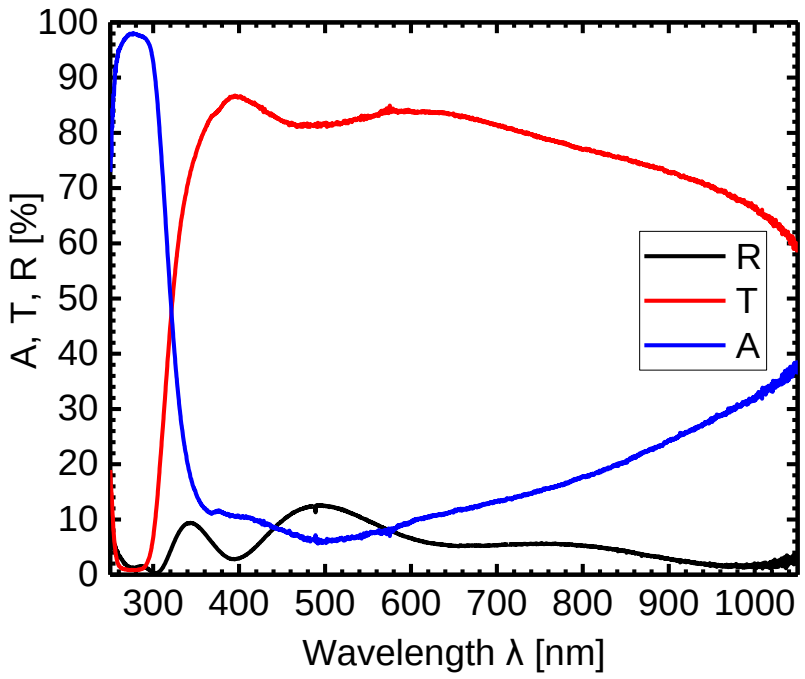

Figure 4.8 ITOglass/ITO/PEDOT:PSS film R, T and A plot.

ITO glass/ITO/ZnO

Figure 4.9 below shows R, T and A plot for ITO glass/ITO/ZnO film.

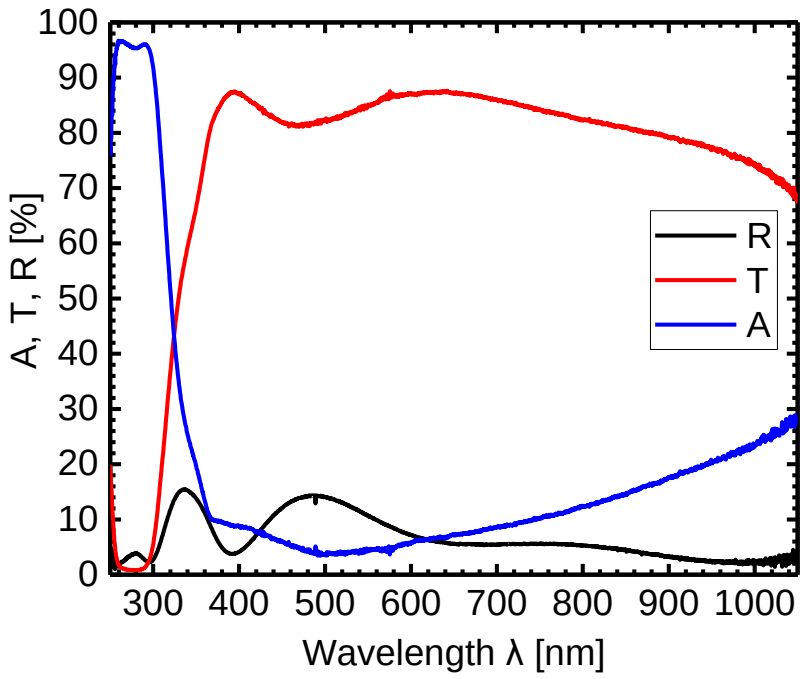

Figure 4.9 R, T and A plot for ITOglass/ITO/ZnO film.

As can be seen above in Figure 4.8 and Figure 4.9, ITO layer is semi-transparent (has T greater than 70%) hence its use as an electrode. ZnO and PEDOT:PSS films have also transmission of almost greater than 70% in the wavelength range of 300 nm to 1100 nm. This is of importance in the use of these materials as they appear in the front of the active layer.

4.1.2.3. Results for Active Layer Films

Figure 4.10 below shows the R, T and a plot for Quartz/PBDB-T film.

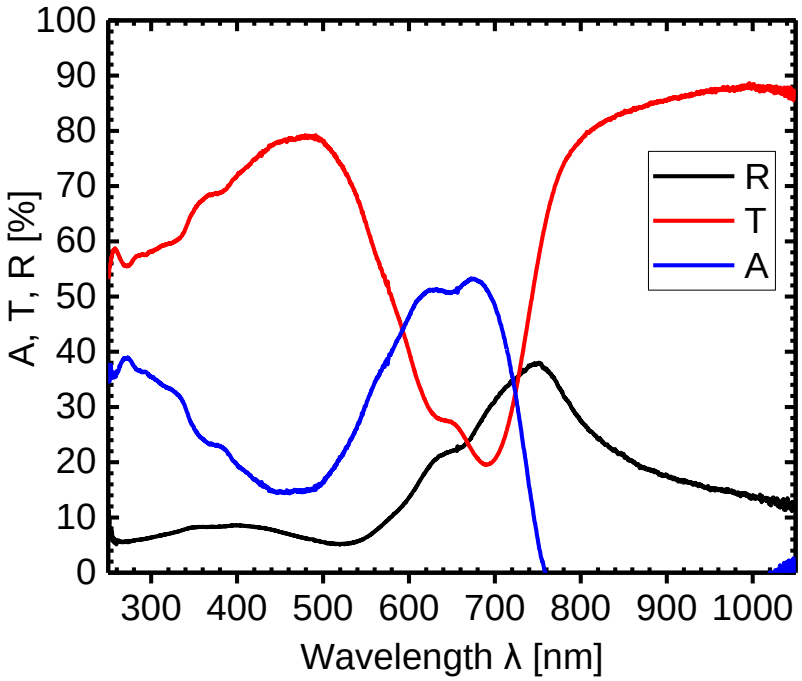

Figure 4.10 Quartz/PBDB-T film R, T and A plot.

Figure 4.11 shows the R, T and a plot for Quartz/ITIC film.

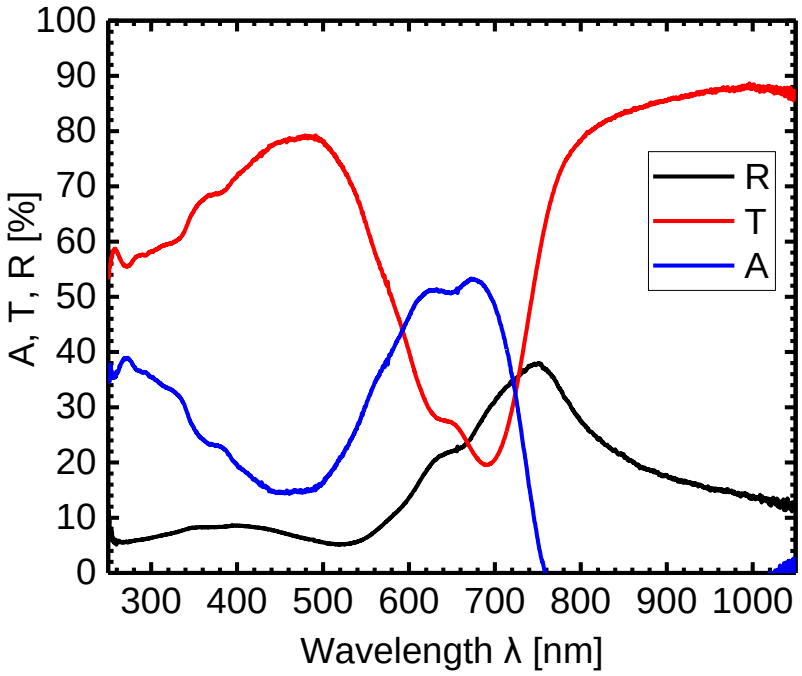

Figure 4.11 Quartz/ITIC film R, T and A plot.

Figure 4.12 below shows the R, T and a plot for Quartz/PBDB-T:ITIC film.

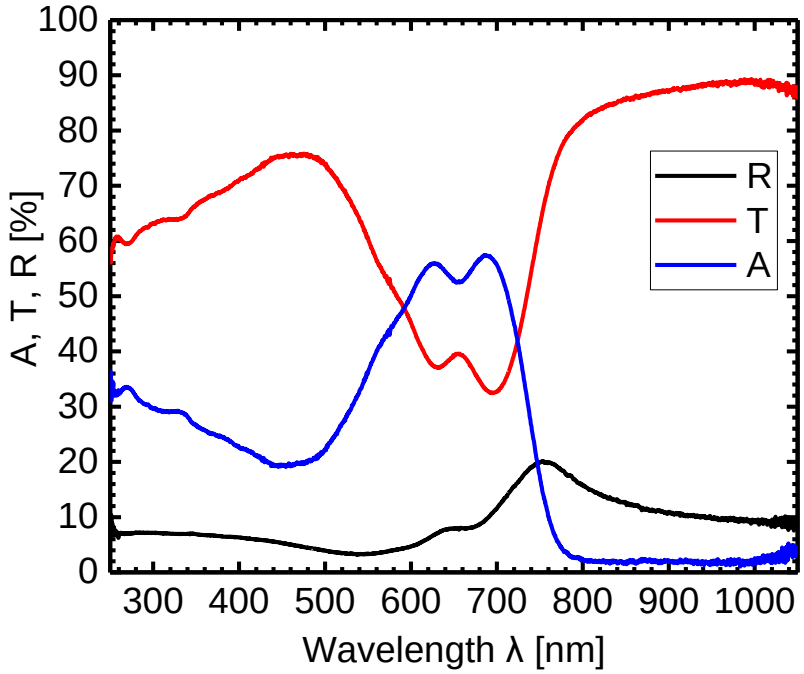

Figure 4.12 Quartz/PBDB-T:ITIC film R, T and A plot.

As can be seen from Figure 4.10, Figure 4.11 and Figure 4.12 above, the materials PBDB-T, ITIC and PBDB-T have almost similar R, T and A properties. All of them have an absorption in the upper wavelength part of the visible region visible region from 550 nm to 750 nm. This is favourable since it is within the solar spectrum range. Of the three materials, the blend PBDB-T:ITIC has the highest absorption in the above specified range.

4.1.2.4. Solar Cells Results

A solar cell with PBDB-T:ITIC active layer was prepared. The layer structure of the solar cell used was Glass/ITO/PEDOT:PSS/PBDB-T:ITIC/Mg/Al. The thicknesses of the solar cell layers were not optimized in order to be able to compare the results with those of the optimized parameters. The approximate thicknesses of the layers were 1.1 nm ITO

glass substrate coated with 140 nm of ITO, 150 nm PEDOT:PSS, 110 nm of PBDB-T:ITIC, 90 nm of Mg and 110 nm of Al layer.

Figure 4.13 below shows the external quantum efficiency of the solar cell prepared.

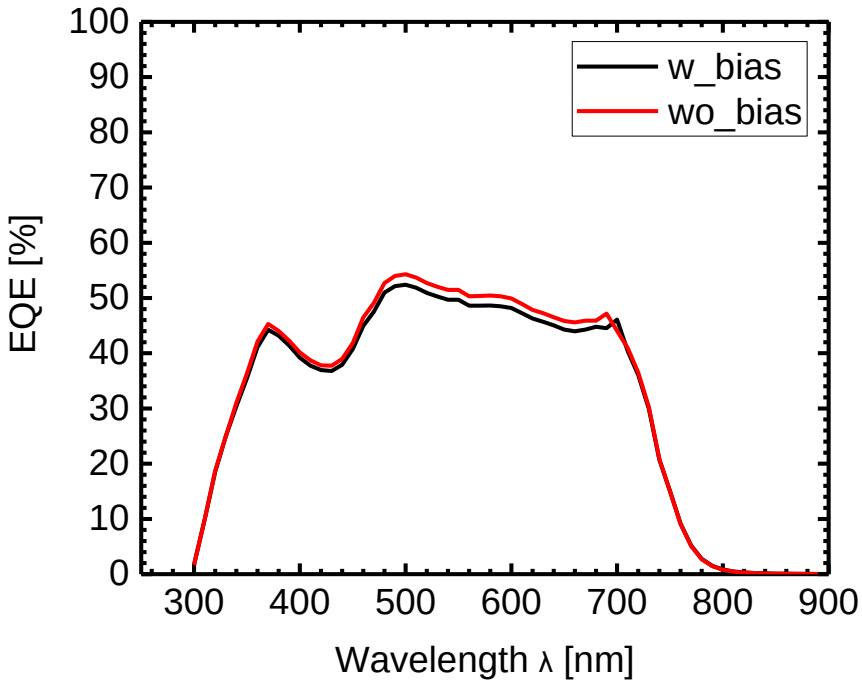

Figure 4.13 External Quantum Efficiency (EQE) of the solar cell showing results for with bias and without bias.

External Quantum Efficiency (EQE) is basically the ratio of the number of charge carriers collected by the solar cell to the number of photons of a given energy shining on the solar cell from outside (incident photons). The EQE of the solar cell was low as its maximum value is around 60 percent. Therefore, about 45 % on average of the incident photons are collected by the solar cell in the region of 350 nm to 750 nm. The low EQE can be attributed to more reflection in the multilayer system due to non-optimized layer thicknesses.

Table 5 below shows the electrical parameters of the solar cell together with the power conversion efficiency. As can be seen, the power conversion efficiency of the solar cell was 4.44% with a fill factor (FF) of 37%. Both the power conversion efficiency and

fill factor are low values and that's why there is need for a simulation of the whole organic solar cell to determine the optimal parameters. It can be seen from these results that the Jsc is averagely high.

Table 5 Results of the solar cell.

Jsc (mA/cm^2)	Voc (mV)	FF (%)	PCE (%)	Rs (Ohm)	Rp (Ohm)	JmPP (mA/cm^2)	VmPP (mV)	Pmax (mW)
14.859	813	37	4.44	26	333	9.25	479.9	1.86

4.2. Optical Modelling Results

In this thesis, optical modelling results consists of the model and measured data fits and output optical constants. Some important parameters can also be extracted from the results such as absorption coefficient and energy loss. Since this thesis is on optical characterization and modelling, the main results will be the n and k values of the films involved in organic solar cell layers. These results consist of graphs for refractive indices (n and k values), dielectric constants, absorption coefficients and other information that can be extracted. Values of all the results can also be exported into an xy data format (nm; n; k). For this work, n and k values were exported into an xy data format and used for the simulation of the whole organic solar cell layer(s). The wavelength range of the data exported was from 250 nm to 1050 nm. Due to the high number of films modelled, only films involved in the layer structure presented in this thesis that is Glass/ITO/PEDOT:PSS/PBDBT:ITIC/Mg/Al will be presented in this subsection. The rest of the results will be presented in the Appendix Section in this thesis.

4.2.1. Substrates

Figure 4.14 below shows the model and measured data for (R and T) for quartz glass alone. For the reflectance and transmittance plots, blue is the model data and red is the imported measured data. For complex refractive index and dielectric function, blue is the real part while red is the imaginary part of the two quantities respectively.

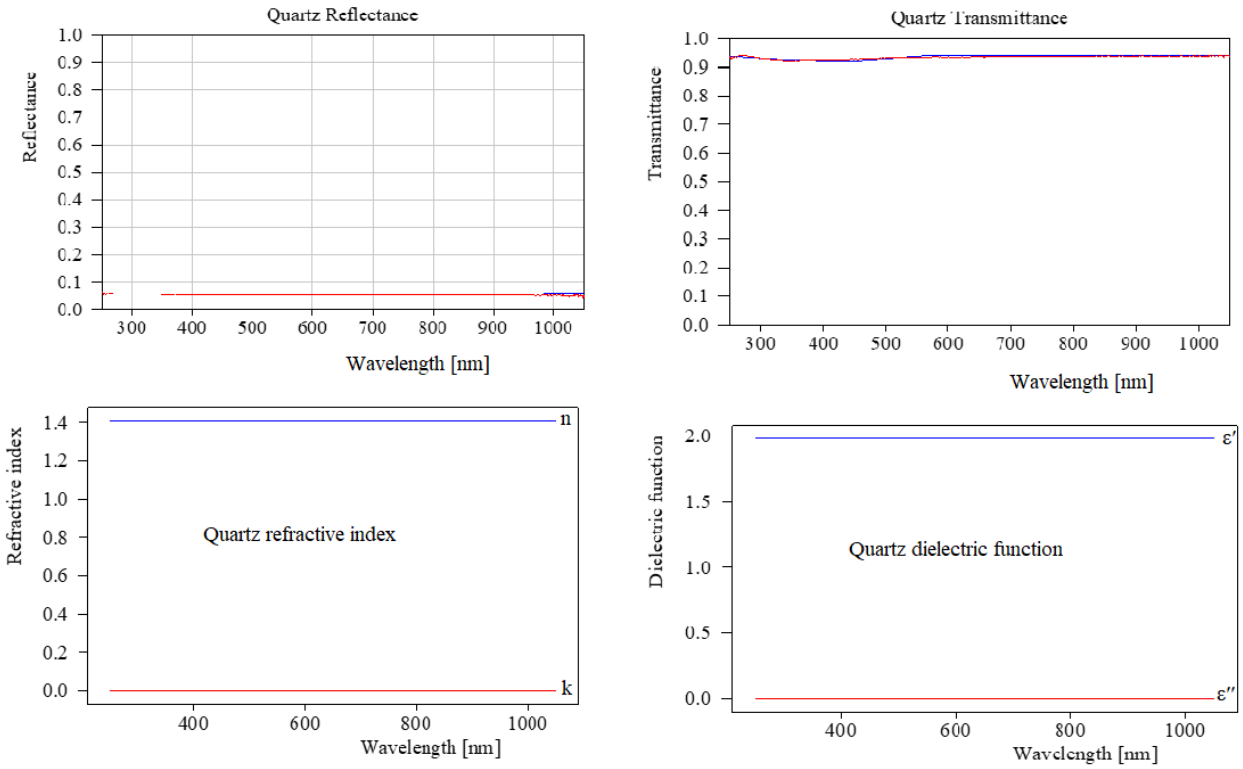

Figure 4.14 Model and measured data for (R and T) for quartz glass substrate alone. For reflection and transmission data blue represents the fit data while red is the experimental data. For the optical constants blue is the real part n while red is the imaginary part of the complex refractive index.

From the result of the fitting in Figure 4.14 above, the good agreement between the model and the experimental data validates the reliability of our proposed method. This can be seen as the fit data is the same as the experimental data. Therefore, the obtained optical constants will resemble the experimental data.

4.2.1.1. Comparison of n and k values for all substrates (quartz, microscope and ITO glass without ITO)

Figure 4.15 below shows results of n and k values for the substrates. Quartz glass substrate has the lowest n value of 1.4 while ITO glass has the highest n value which starts from 1.48 to 1.55. This means that quartz glass is the most transparent among all these substrates since the lower the n value the more transparent the substrate is. For all these substrates the extinction coefficient (k) is almost zero.

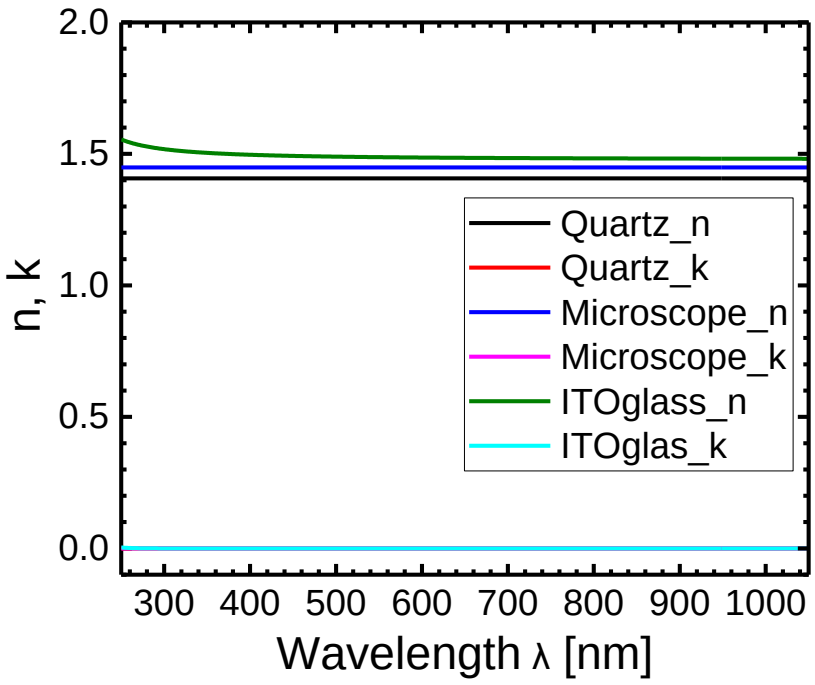

Figure 4.15 Comparison of n and k values for quartz, microscope and ITO glass without ITO (etched ITO glass).

4.2.1.2. Comparison of results from R only and results from using both R and T for fitting

Figure 4.16 below shows the n and k values for Quartz glass. For one pair of n and k, Reflection only was used to produce the model while for the other pair both Reflection and Transmission were used to obtain the model dielectric functions. Using R only gives gives an average n of 1.40 while using both R and T gives an average n of 1.45 as shown in Figure 4.16 below. Therefore, an error of about 3.5% is observed due to using R only for modelling quartz glass. This is likely to increase in materials that have more varying n and k values against the wavelength. The error however differs depending on material. In general, in order to get accurate results both reflection and transmission measured data should be used.

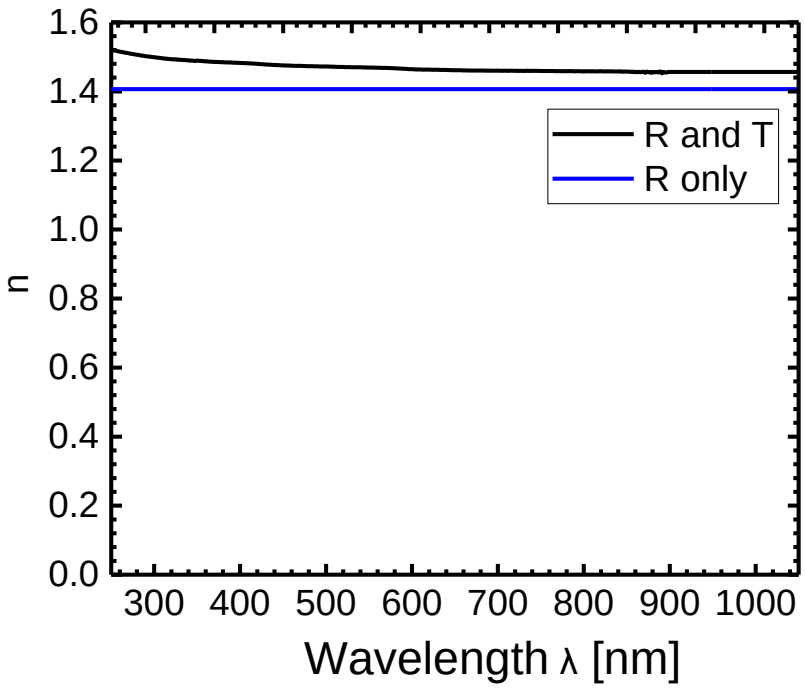

Figure 4.16 Comparison of fitted data with using Reflection only and the other one using Reflection and Transmission.

4.2.2. Metals and Metal Oxide Films

Figure 4.17 below shows the fitted and measured data for (R and T) for PEDOT:PSS films on quartz glass. For the reflectance and transmittance plots, blue is the fit data and red is the imported measured data. For complex refractive index and dielectric function, blue is the real part while red is the imaginary part of the two quantities respectively. Figure 4.18 below shows the n and k values for PEDOT:PSS film on quartz substrate glass together with the complex dielectric functions.

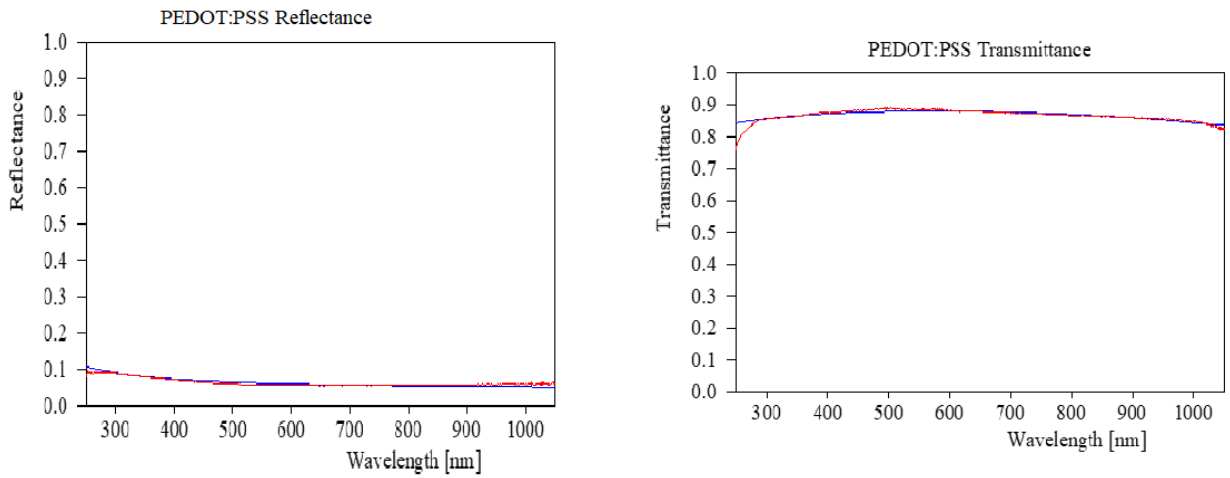

Figure 4.17 Model and measured R and T data for PEDOT:PSS film on Quartz glass. For reflection and transmission data blue represents the fit data while red is the experimental data. For the optical constants blue is the real part n while red is the imaginary part of the complex refractive index.

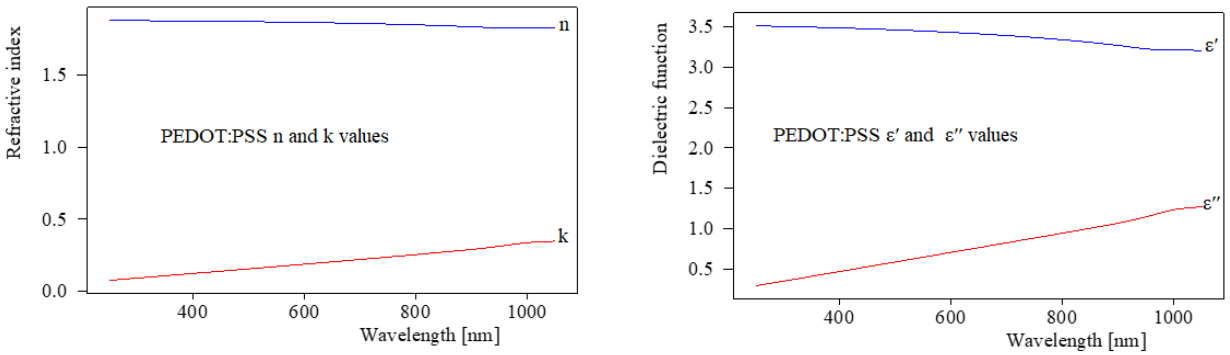

Figure 4.18 Optical constants of PEDOT:PSS film on quartz glass.

4.2.3. Active Layer Films

Optical constants of the PBDB-T:ITIC were also obtained. In order to do that the reflection and transmission measurements of PBDB-T, ITIC and PBDB-T:ITIC films were used to model dielectric functions of the films. Figure 4.19 below shows the fit and experimental data for PBDB-T:ITIC reflection and transmission done in CODE software.

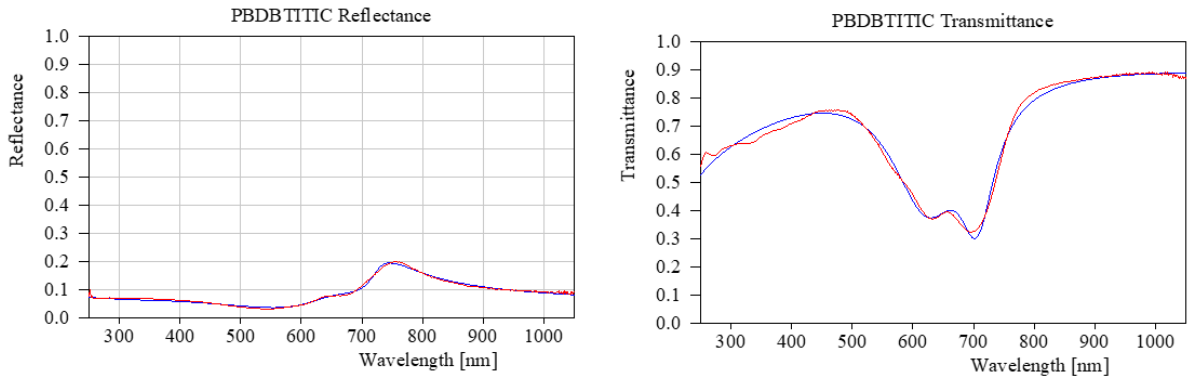

Figure 4.19 R and T Fit and experimental data for PBDB-T:ITIC film on quartz substrate glass. Blue is the fit data while red is the experimental data.

Figure below shows the dielectric functions of the PBDB-T:ITIC film.

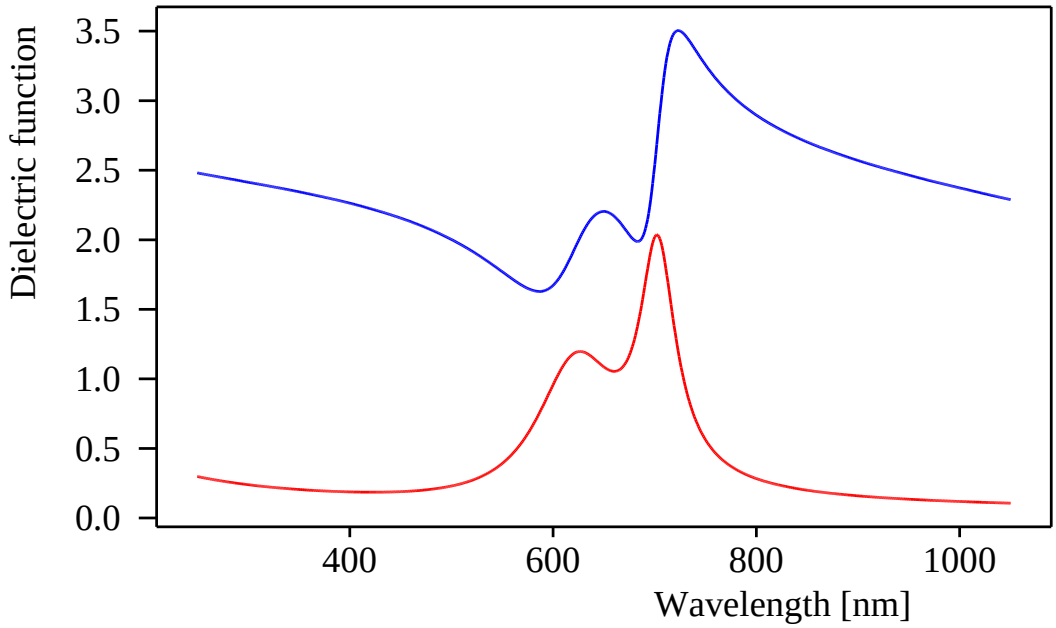

Figure 4.20 Complex dielectric functions for PBDB-T:ITIC film. Blue is the real part while red is the imaginary part of the complex dielectric function.

For the reflection the fit data (model) is in agreement with the experimental data. However, for the transmission there are slight differences between the fit data and the experimental transmission data. From Figure 4.19 data, optical constants were extracted for the PBDB-T:ITIC film. Figure 4.21 below shows the

plot of n and k values for PEDOT:PSS, ITO layer and PBDB-T:ITIC films. From the fitting of the modelling the fitted thickness of PBDB-T:ITIC film was 117 nm. This means that a thickness of around 117 nm will likely bring good results when fabricating the PBDB-T:ITIC based organic solar cells.

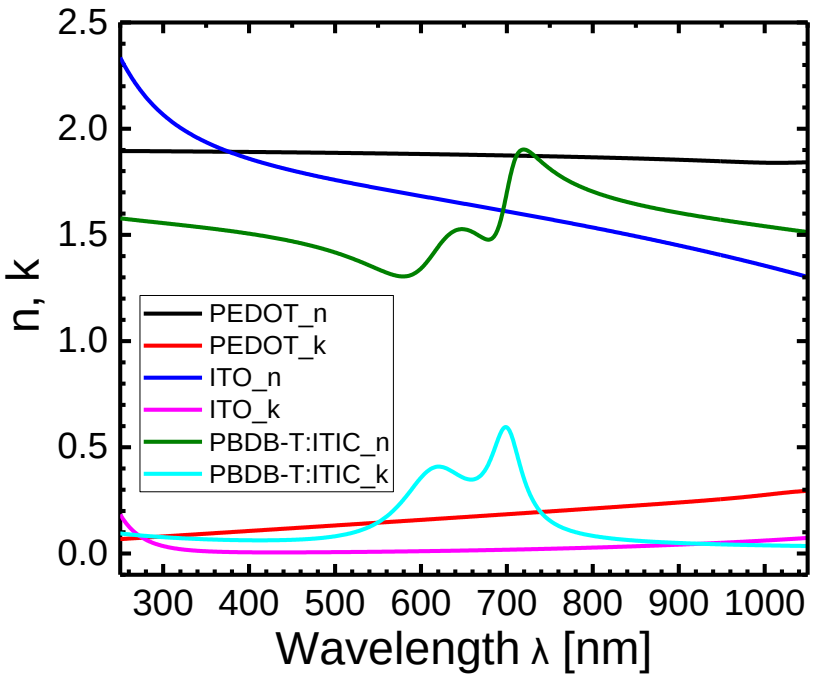

Figure 4.21 n and k values for PEDOT:PSS, ITO layer and PBDB-T:ITIC films.

It can be seen from Figure 4.21 above that PEDOT:PSS has n value of 1.85 on average. ITO has an n value that decreases with increasing wavelength. All these layers are found in front of the photoactive layer in an organic solar cell layer structure. Besides their respective functionalities they all are transparent meaning they do not interfere much with the incoming light before it reaches the photoactive layer where absorption will happen for current to be generated.

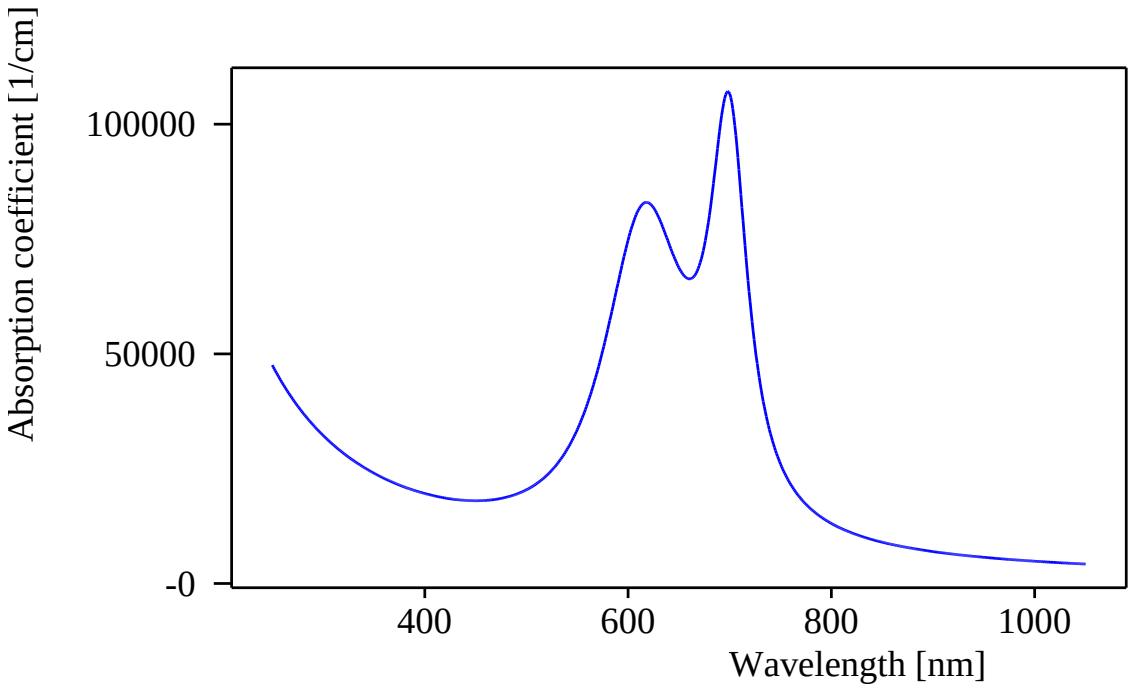

Figure 4.22 Absorption coefficient of PBDB-T:ITIC

Absorption coefficient is a parameter that is used to quantify absorption of light by an optical medium. As can be seen in Figure 4.22, PBDB-T:ITIC has a strong absorption in the region between 600 nm and 800 nm. This region happens to fall on the part of the solar absorption spectrum. However low absorption of the PBDB-T:ITIC in the region from 300 nm to 500 nm is not favourable to the organic solar cell.

4.2.3.1. Comparison of n and k values for metal electrodes

Figure 4.23 below shows n and k plot for Al, Ag, Mg/Al together with Mg films.

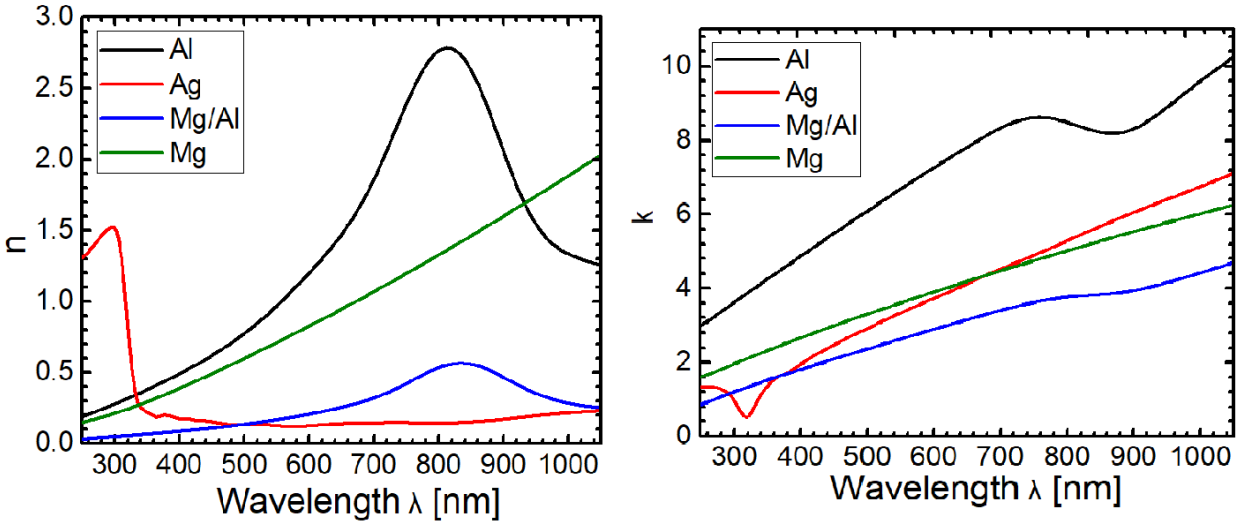

Figure 4.23 n and k values for metals used in organic solar cells.

From Figure 4.23 it can be seen that its either the metal have n lower than 1 or highly higher than 1. All of the metal films have k values increasing with increasing wavelength.

4.2.4. Bruggeman's Effective Medium Approach Results

The Bruggeman's effective medium approach was used to estimate the n and k values of PBDB-T:ITIC from the individual n and k values of PBDB-T and ITIC. Figure 4.24 below shows the results of Bruggeman approach. Since the volume ration of the materials in PBDB-T:ITIC is 1:1, either of PBDBT or ITIC could be taken as the matrix material or the particle material. For results shown below ITIC was the matrix material and PBDB-T:ITIC as the particle material.

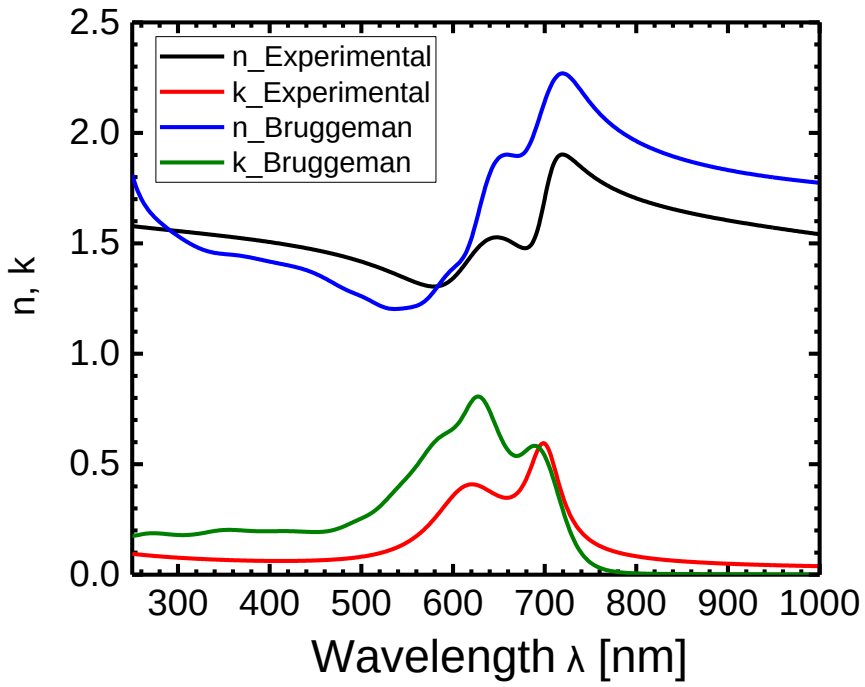

Figure 4.24 n and k results of the Bruggeman's effective medium approach on PBDB-T:ITIC. The volume ration of PBDB-T as to ITIC was 1:1 for both the experimental and the Bruggeman calculation method.

The Bruggeman's approach n and k results are slightly different to the experimental ones. Differences are assumed to be rising from the errors in fitting the PBDB-T and ITIC films as there were slight differences between the model and the experimental data. Since the errors come from two materials, their combined result will be magnified.

From the results of the Bruggeman estimation, it can be seen that the approach has an accuracy of when compared to the CODE software approach (using experimental data) of finding the optical constants of PBDB-T:ITIC using R and T measurements. Furthermore, by changing the volume ratio of the active layer constituent materials, the approximate n and k values of the composite active layer material were obtained. For example, when the ration of PBDB-T and ITIC is 1:1, the following are the n and k values of the PBDB-T:ITIC composite material formed.

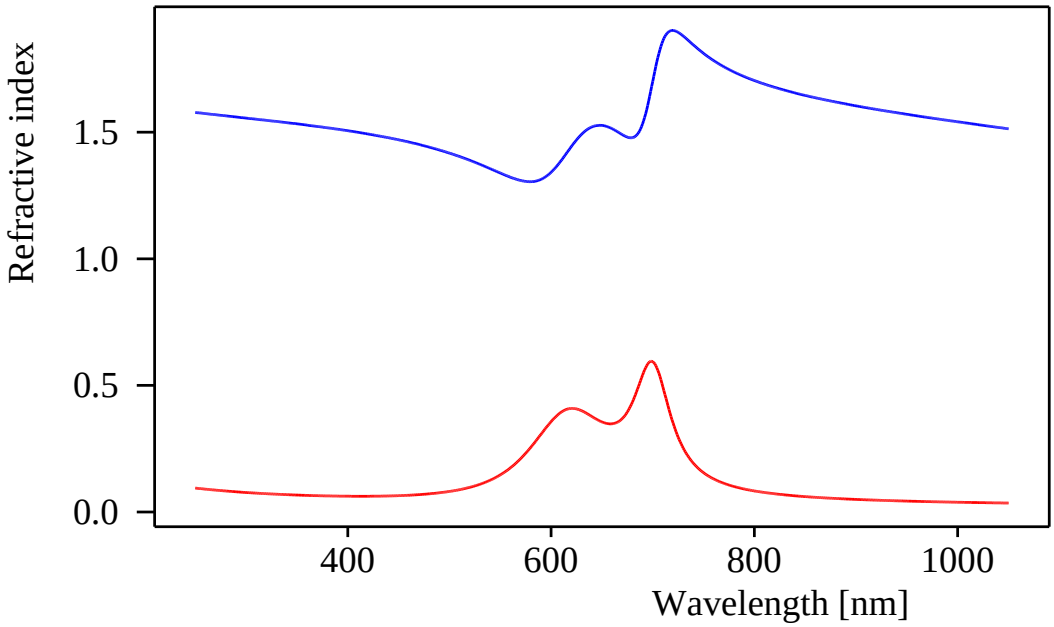

Figure 4.25 n and k values of the blend PBDB-T:ITIC layer with 1:1 volume ratio.

By changing the volume ratio of the materials using the Bruggeman approach integrated in CODE software, the respective n and k values of the blend were determined. This is a faster way of determining optical constants of the blend from the respective optical constants of the constituent materials.

4.3. Simulation Results

The following are the results of the simulation of an organic solar cell multilayer. The layer structure of the solar cell used was Glass/ITO/PEDOT:PSS/PBDB-T:ITIC/Mg/Al. The thickness of the active layer was varied from 10 nm to 300 nm and the Mathematica simulation was done in one run producing the results for 2 nm steps. Key parameters for each thickness were maximum current density, EQE values, maximum power and number of photons generated. From the simulation results the following were the results.

Figure 4.26 below shows variation of current density with thickness for the simulated solar cell. The thickness was varied from 10 nm to 300 nm calculating the respective current density for each thickness. It can be seen below that the current density increases

with increase in thickness. One of the main design challenges for thin-film solar cells is to find the ideal absorber thickness that represents the best compromise between strong light absorption and efficient charge carrier collection [41]. The best active layer thickness should represent both strong light absorption and efficient charge carrier collection.

Following the curve of the graph in Figure 4.26 it can be seen that from 10 nm to around 150 nm, as thickness was increased, respective maximum current density was increasing correspondingly. However, after 150 nm current density was not increasing that much after an increase in thickness. Therefore 150 nm can be taken as a good optimal thickness for the active layer following the arguments on balancing light absorption and charge carrier collection described above. From the 150 nm thickness the maximum current density obtained was 24 mA/cm^2. Comparing this to the 14 mA/cm^2obtained in the solar cell fabricated, it will be seen that there is still room for improving the solar cell using the parameters from the simulation.

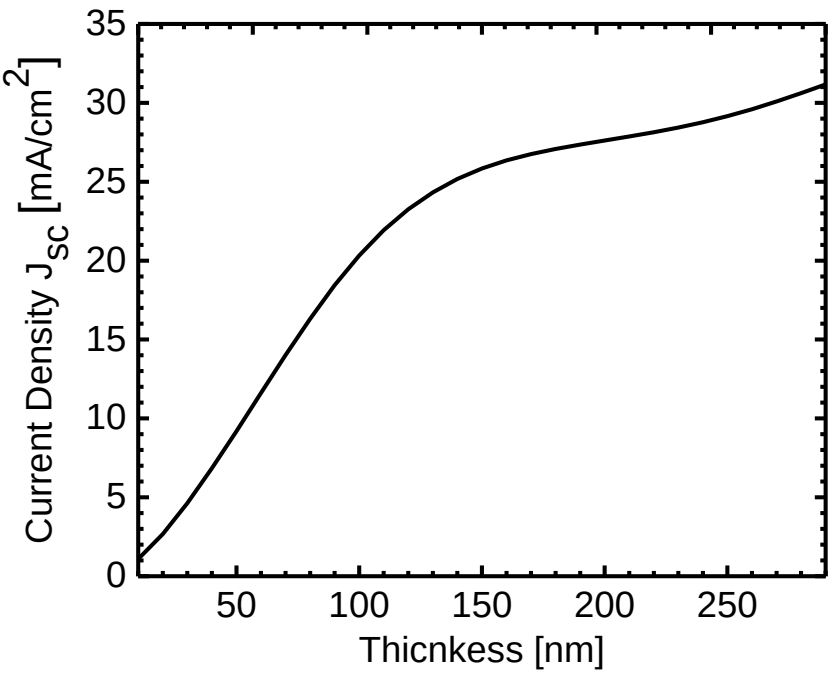

Figure 4.26 Variation of current density with thickness for the simulated solar cell.

Figure 4.27 below also shows the EQE plot using the results from the simulation. Through the transfer matrix formalism, it was possible to simulate the whole organic solar

cell from the glass substrate to the Al layer. Absorption in the active layer was also determined for each respective active layer thickness.

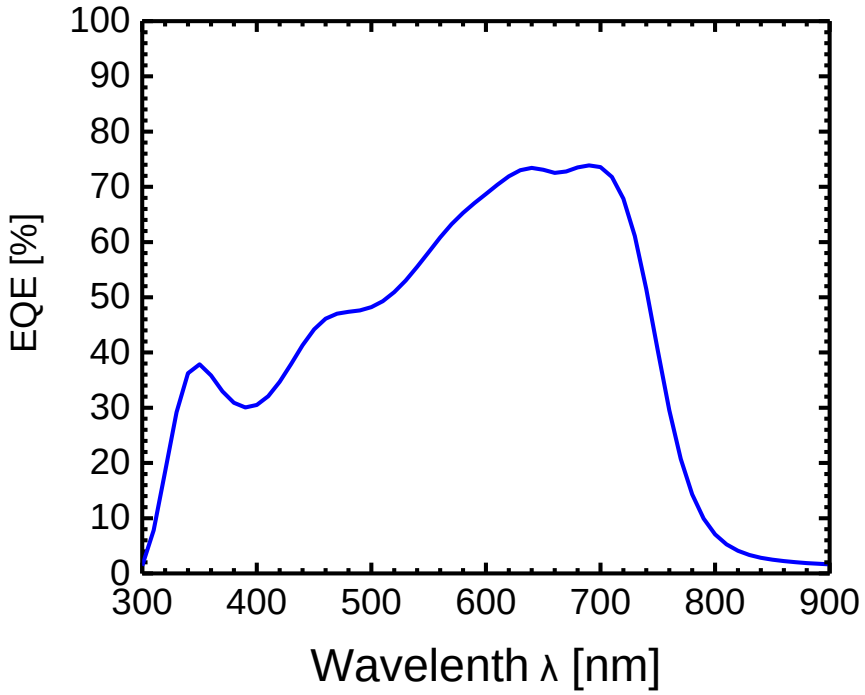

Figure 4.27 Simulated EQE for the solar cell with thickness of 90 nm.

The simulated EQE is above 60% from 600 nm to 730 nm. In all the other regions the EQE is slightly above 50%. From the 150 nm thickness the maximum current density obtained was 24 mA/cm^2. Comparing this to the 14 mA/cm^2obtained in the solar cell fabricated, it will be seen that there is still room for improving the solar cell using the parameters from the simulation.

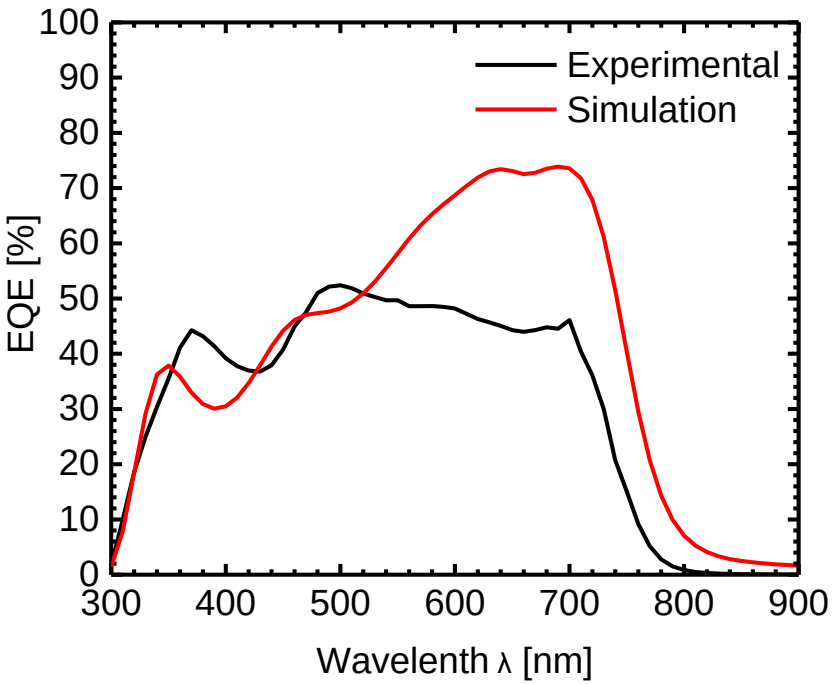

Figure 4.28 Simulated and experimental EQE. Note: The experimental EQE is of the solar cell without optimization. The simulated EQE uses optimized parameters such as active layer film thickness.

It can be seen from Figure 4.28 that the simulated EQE is better than the experimental especially from 500 nm to 800 nm range. Highest EQE recorded was 73 %. From 800 nm, the EQE becomes almost zero. This is because the EQE follows the absorption of the PBDBT:ITIC active layer where after 800 nm the absorption becomes zero. There are improvements that can be made by using the optimal parameters obtained from the simulation. These include using the optimal thickness especially of the active layer.

5. SUMMARY AND CONCLUSION

From the Results Section, it can be seen that different materials for organic solar cells have different optical constants and the same n and k values can be used to uniquely describe the materials. The optical constants were obtained from the reflection and transmission measurements. Reflection and transmission measurements were done for each layer followed by the extraction of n and k values through modelling dielectric functions of the respective films. The optical modelling results were used for simulating the whole organic solar cell using the transfer matrix formalism. From the simulation, maximum internal quantum efficiency, maximum current density and the optimized active layer thickness together with other information pertaining the organic solar cell studied were obtained. Through use of the Bruggeman's effective medium approach the optical constants for PBDB-T:ITIC were determined from the optical constants of PBDB-T and ITIC films. By changing the blend ratio of PBDB-T:ITIC, the respective n and k values of PBDB-T:ITIC blend were determined through a faster and accurate method.

Besides its use in organic solar cells, modelling and simulation of optical quantities like total transmittance, reflectance and internal light absorption is very useful in fields such as optical coating design, thin film optimization and measurement systems, interferometric absorber and emitter designs.

REFERENCES

1. IEA, *World Energy Outlook 2017*. 2017, International Energy Agency (IEA). p. 32.
2. Tom, M. and L. Castañer, *PRACTICAL HANDBOOK OF PHOTOVOLTAICS: FUNDAMENTALS AND APPLICATIONS.* Elsevier, 2012.
3. Yeh, N. and P. Yeh, *Organic solar cells: Their developments and potentials.* Renewable and Sustainable Energy Reviews, 2013. **21**: p. 421-431.
4. Hoppe, H. and N.S. Sariciftci, *Polymer Solar Cells.* 2007: p. 1-86.
5. Kallmann, H. and M. Pope, *Photovoltaic Effect in Organic Crystals.* The Journal of Chemical Physics, 1959. **30**(2): p. 585-586.
6. Berger, P.R. and M. Kim, *Polymer solar cells: P3HT:PCBM and beyond.* Journal of Renewable and Sustainable Energy, 2018. **10**: p. 27.
7. Li, N., et al., *Towards 15% energy conversion efficiency: a systematic study of the solution-processed organic tandem solar cells based on commercially available materials.* Energy & Environmental Science, 2013. **6**(12): p. 3407-3413.
8. Cui, Y., et al., *Fine-Tuned Photoactive and Interconnection Layers for Achieving over 13% Efficiency in a Fullerene-Free Tandem Organic Solar Cell.* J Am Chem Soc, 2017. **139**(21): p. 7302-7309.
9. Griffith, M.J., et al., *Roll-to-Roll Sputter Coating of Aluminum Cathodes for Large-Scale Fabrication of Organic Photovoltaic Devices.* Energy Technology, 2015. **3**(4): p. 428-436.
10. Alaibakhsh, H. and G. Darvish, *Optical modeling of sunlight by using partially coherent sources in organic solar cells.* Applied Optics, 2016. **55**(7): p. 1808-1813.
11. Min, X., et al., *Polyethylenimine aqueous solution: a low-cost and environmentally friendly formulation to produce low-work-function electrodes for efficient easy-to-fabricate organic solar cells.* ACS Appl Mater Interfaces, 2014. **6**(24): p. 22628-33.
12. Hecht, E., *Optics*. Vol. 5th. Pearson.
13. Peatross, J. and M. Ware, *Physics of Light and Optics*. 2008: Brigham Young University.
14. Dresselhaus, M.S., *Optical Properties of Solids*. Vol. 2. 1999.
15. Flammer, J., M. Mozaffarieh, and H. Bebie, *The Interaction Between Light and Matter.* 2013: p. 21-39.
16. Feng, M.Q., G. Roqueta, and L. Jofre, *Non-destructive evaluation (NDE) of composites: microwave techniques.* 2013: p. 574-616.
17. Jenkins, F. and H.E. White, *Fundamentals of Optics*. 2001, New York: McGraw-Hill Higher Education.
18. Cardona, M. and P.Y. Yu, *Optical Properties of Semiconductors.* Material Science, 2011. **2**.
19. Hung, K.-Y. and J.-C. Liao, *The application of Fresnel equations and anti-reflection technology to improve inclined exposure interface reflection and develop a key component needed for Blu-ray DVD–micro-mirrors.* Journal of Micromechanics and Microengineering, 2008. **18**(7): p. 075022.
20. Harbecke, B., *Coherent and incoherent reflection and transmission of multilayer structures.* Applied Physics B, 1986. **39**(3): p. 165-170.
21. Gupta, Y. and P. Arun, *First Step to Ellipsometry.* International Journal of Physics, 2015. **3**(1): p. 8-11.

22. Hu, B.Y.K., *Kramers–Kronig in two lines.* American Journal of Physics, 1989. **57**(9): p. 821-821.
23. Buffeteau, T. and B. Desbat, *Thin-Film Optical Constants Determined from Infrared Reflectance and Transmittance Measurements.* Applied Spectroscopy, 1989. **43**(6): p. 1027-1032.
24. Song, Q.L., et al., *Optical interference effect in layered organic materials studied by UV–Vis absorption spectroscopy.* Journal of Luminescence, 2006. **119-120**: p. 142-147.
25. Hoppe, H., et al., *Modeling the optical absorption within conjugated polymer/fullerene-based bulk-heterojunction organic solar cells.* Solar Energy Materials and Solar Cells, 2003. **80**(1): p. 105-113.
26. Hoppe, H., *OPTICAL CONSTANTS OF CONJUGATED POLYMER/FULLERENE BASED BULK-HETEROJUNCTION ORGANIC SOLAR CELLS.* 2002. **385**.
27. Lenze, M.R., et al., *Determination of the optical constants of bulk heterojunction active layers from standard solar cell measurements.* Organic Electronics, 2014. **15**(12): p. 3584-3589.
28. Bruggeman, D.A.G., *Berechnung verschiedener physikalischer Konstanten von heterogenen Substanzen. I. Dielektrizitätskonstanten und Leitfähigkeiten der Mischkörper aus isotropen Substanzen.* Annalen der Physik, 1935. **416**(7): p. 29.
29. QiYing, L., *Convenient and inexpensive determination of optical constants and film thickness of blended organic thin film.* Physics, Mechanics and Astronomy, 2015. **58**.
30. Pettersson, L.A.A., L.S. Roman, and O. Inganas, *Modeling photocurrent action spectra of photovoltaic devices based on organic thin films.* Journal of Applied Physics, 1999. **86**(1): p. 487-496.
31. Monestier, F., et al., *Optical modeling of organic solar cells based on CuPc and C_60.* Applied Optics, 2008. **47**(13): p. C251.
32. Zhang, Z., et al., *Energy-level modulation of non-fullerene acceptors to achieve high-efficiency polymer solar cells at a diminished energy offset.* Journal of Materials Chemistry A, 2017. **5**(20): p. 9649-9654.
33. Liu, Q., et al., *High open-circuit voltage and short-circuit current flexible polymer solar cells using ternary blends and ultrathin Ag-based transparent electrodes.* Journal of Materials Chemistry A, 2017. **5**(48): p. 25476-25484.
34. Morita, N., K. Torizuka, and T. Yajima, *Coherent propagation effect of incoherent light.* Journal of the Optical Society of America B, 1986. **3**(4): p. 548-553.
35. Theiss, W. *Scout Technical Manual*. 2013.
36. Kim, C.C., et al., *Modeling the optical dielectric function of semiconductors: Extension of the critical-point parabolic-band approximation.* Physical Review B, 1992. **45**(20): p. 11749-11767.
37. Stroud, D., *The effective medium approximations: Some recent developments.* Superlattices and Microstructures, 1998. **23**(3-4): p. 567-573.
38. Khardani, M., M. Bouaïcha, and B. Bessaïs, *Bruggeman effective medium approach for modelling optical properties of porous silicon: comparison with experiment.* physica status solidi (c), 2007. **4**(6): p. 1986-1990.
39. Schmidt, D. and M. Schubert, *Anisotropic Bruggeman effective medium approaches for slanted columnar thin films.* Journal of Applied Physics, 2013. **114**(8): p. 083510.

40. Gordillo-Vazquez, F.J., *An effective-medium approach to the optical properties of heterogeneous materials with nonlinear properties.* Journal of Modern Optics, 2003. **50**(1): p. 113-135.
41. Kirchartz, T., et al., *Understanding the Thickness-Dependent Performance of Organic Bulk Heterojunction Solar Cells: The Influence of Mobility, Lifetime, and Space Charge.* The Journal of Physical Chemistry Letters, 2012. **3**(23): p. 3470-3475.

APPENDIX A

Characterization results

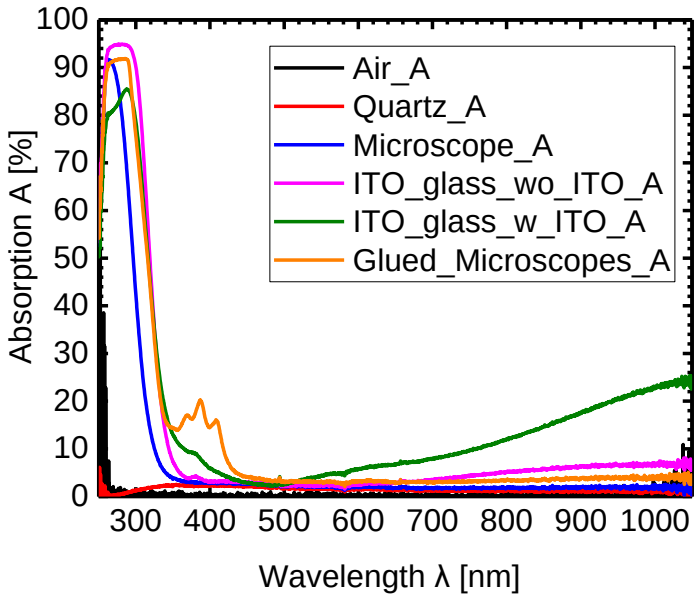

Figure 5.1 Absorption comparison for substrates glass

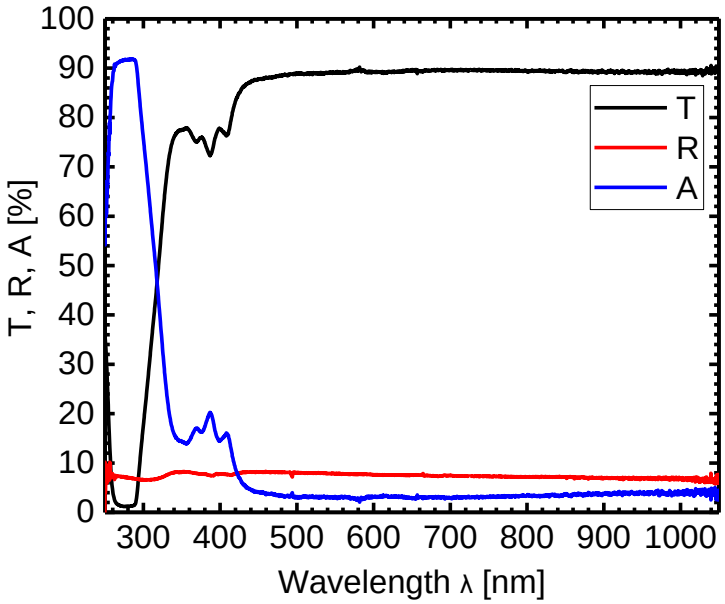

Figure 5.2 Glued Microscope glass R, T and A plot.

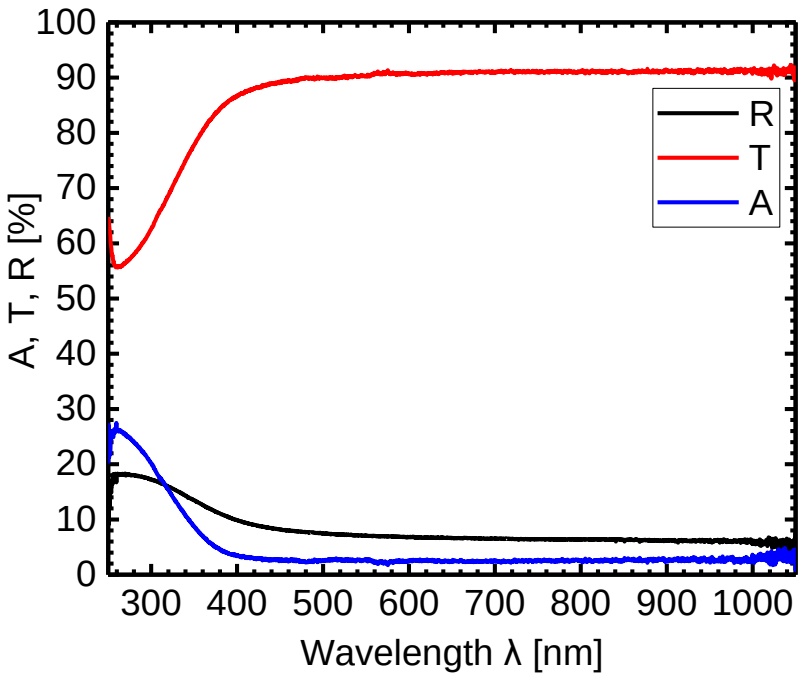

Figure 5.3 Quartz/MoO_3 film R, T and A plot.

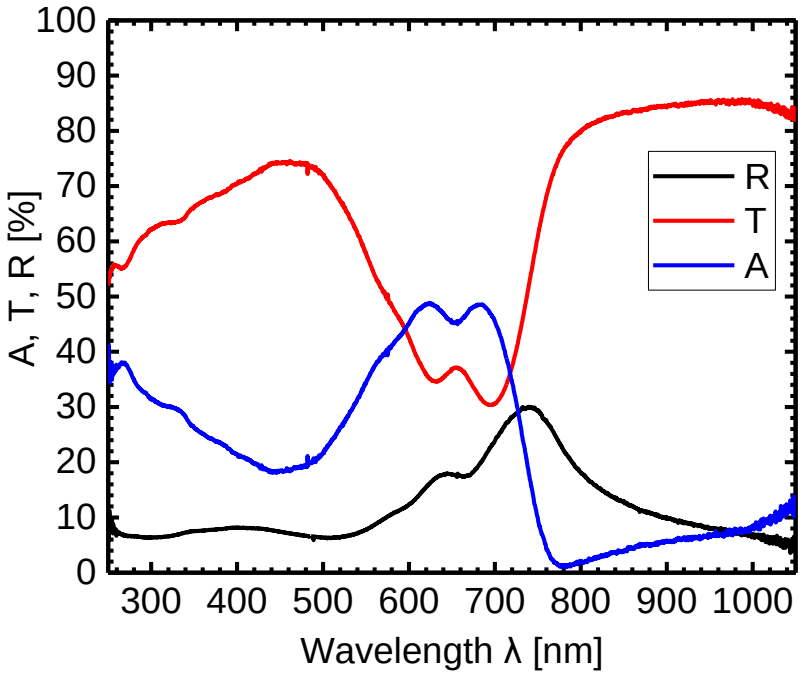

Figure 5.4 Quartz/PEDOT:PSS/PBDB-T:ITIC

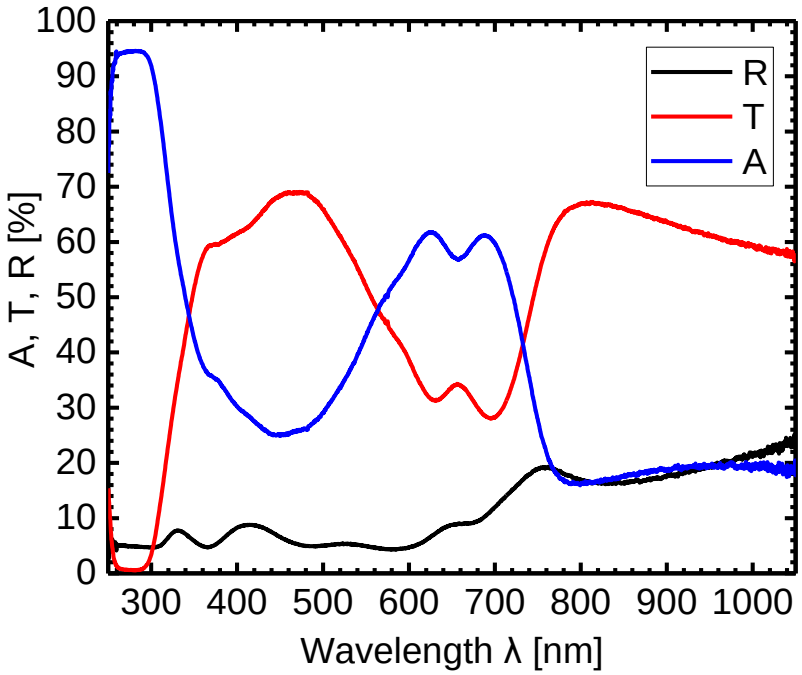

Figure 5.5 ITO glass/ITO/ZnO/PBDB-TITIC

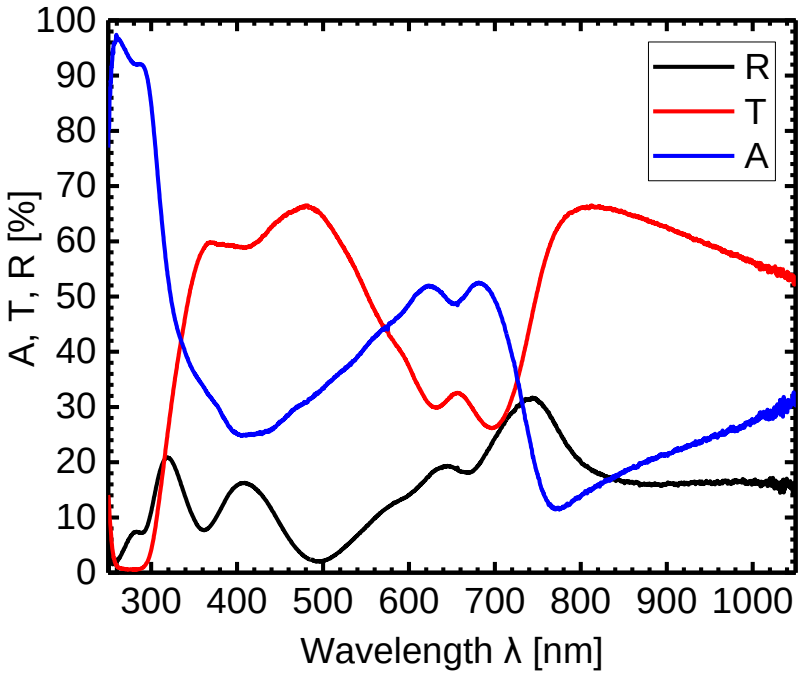

Figure 5.6 ITO glass/ITO/PEDOT:PSS/PBDB-T:ITIC

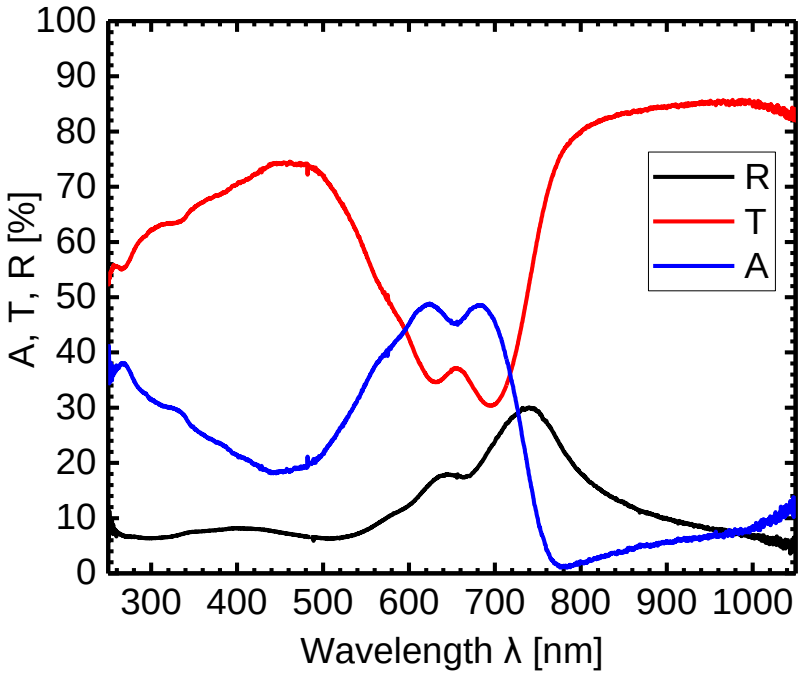

Figure 5.7 Quartz/PEDOT:PSS/PBDB-T:ITIC

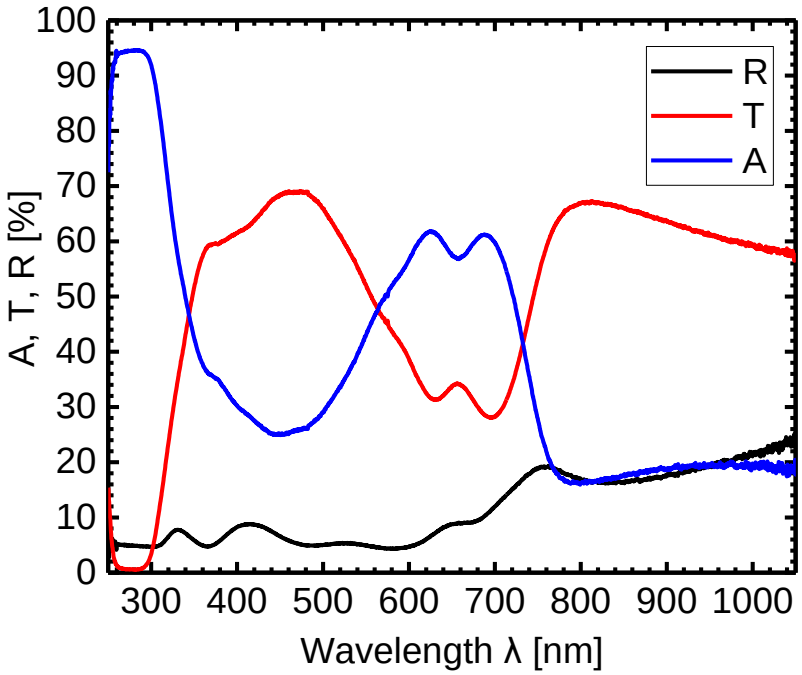

Figure 5.8 ITO glass/ITO/ZnO/PBDB-TITIC

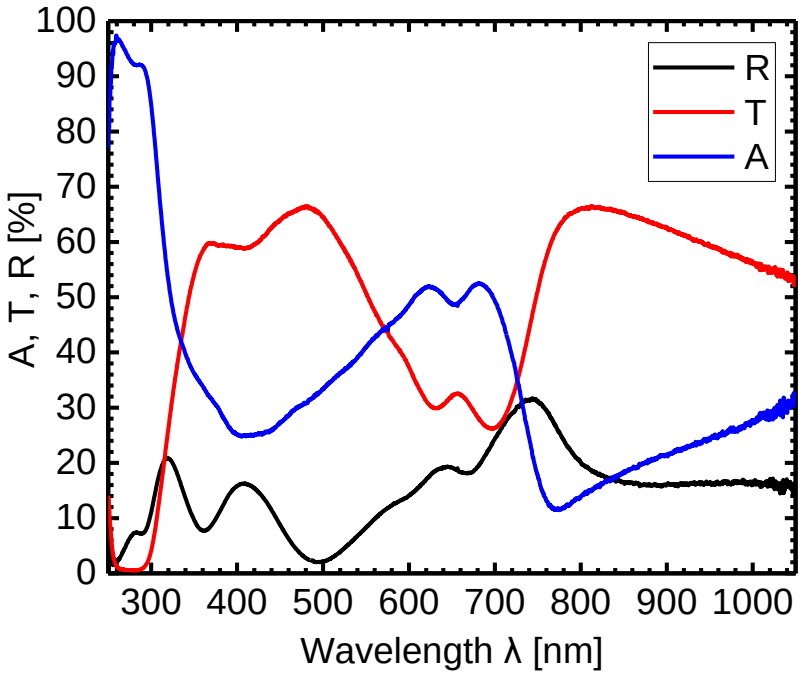

Figure 5.9 ITO glass/ITO/PEDOT:PSS/PBDB-T:ITIC

APPENDIX B

Film thickness measurement results using Atomic Force Microscopy (AFM)

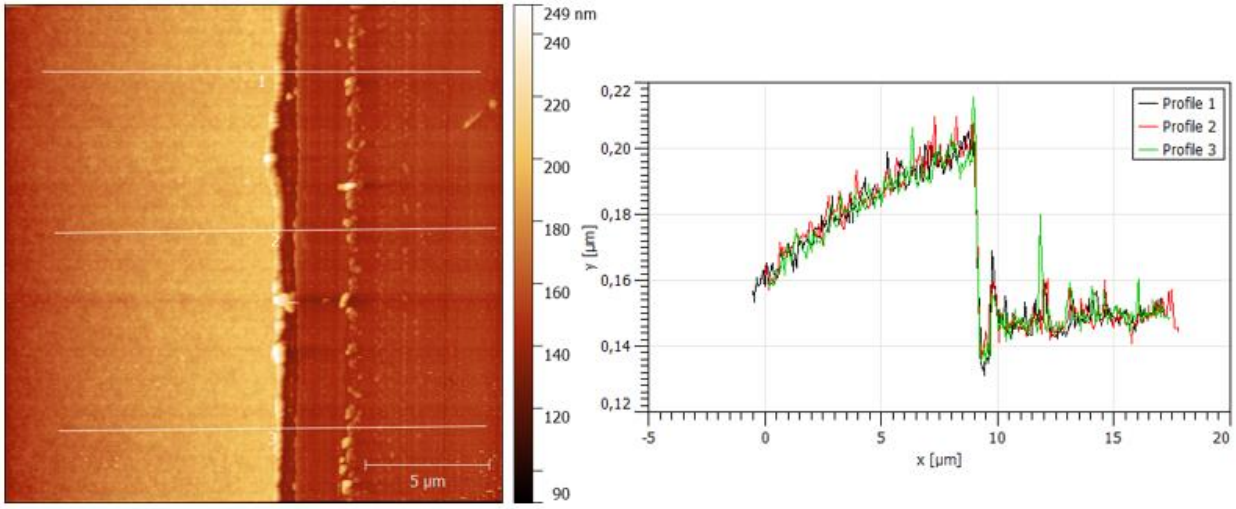

Figure 5.10 Film thickness measurement for PBDBT:ITIC using Atomic Force Microscopy (AFM). The thickness of the film was found to be 80 nm.

APPENDIX C

Expenses incurred by the student

Expenses

Table 1 below shows the expenses made by Zvirevo Chisadza for the realisation of the thesis.

Table 1. Expenses made by the student

Item	Description	Quantity	Unit Cost (Euro)	Total Cost (Euro)
Visa Processing				
Total costs	For Germany Visa	Many	80	80
Travel Costs				
Flight Costs	Algeria to Germany return ticket	1	400	400
Tlemcen to Algiers	Tlemcen to Algiers to and from	1	40	40
Train to Jena	Frankfurt to Jena	1	70	70
Train From Jena	Jena to Frankfurt	1	30	30
Living Requirements				
Accommodation	For months + services	6	306.50	1839
Local transport	For 5 months	5	44	220
Services Required				
Travel and Health insurance	For health from Algeria	1	90	90
Liability Insurance	For Germany	1	60	60

Health Insurance Germany	In Germany	1	70.71	70.71
Student Thoska card	Student registration	1	10	10
Other costs	Travel for Research	1	26	26
			TOTAL	**2 935.71**

Equivalent Amount in USD Dollars: **$3 669.64**

Signatures:

Date 29.08.18 Place Jena, Ciermany

Superviser: Dr. Harald Hoppe

Student: Zvirevo Chisadza